

Subharmonic resonance and critical eccentricity for the classical hydrogen atomic system

D Cole. "Subharmonic resonance and critical eccentricity for the classical hydrogen atomic system." *European Physical Journal D*,
<https://hdl.handle.net/2144/29982>

"Downloaded from OpenBU. Boston University's institutional repository."

Subharmonic resonance and critical eccentricity for the classical hydrogen atomic system

Daniel C. Cole

Boston University, Mechanical Engineering Dept.
110 Cummington Mall, Boston, MA 02215
dccole@bu.edu

March 24, 2018

Abstract

Subharmonic resonance behaviors are investigated for the classical hydrogen atom, with classical radiation damping and circularly polarized light acting on the classical electron. This study is intended for both potential experimental applications as well as for deeper theoretical purposes. Long resonant states are predicted for realistic Rydberg atoms and highly excited hydrogen states. Several previously undiscovered physical effects are predicted. First, the semimajor axis remains relatively constant when in subharmonic resonance; second, the eccentricity steadily increases until a maximum, critical value is reached, at which point orbital decay sets in. If the initial orbit is circular, this critical eccentricity value is shown to always be the same for each subharmonic condition, regardless of the initial orbital radius. An analytic derivation for this result is presented. The illustrated dynamics are of interest for the classical theory of stochastic electrodynamics (SED) regarding whether SED can fundamentally describe more of quantum phenomena, particularly atomic excited state behavior and related emission and absorption spectra. Also of interest are how classical resonances can be imposed on a near continuum of quantum states. Finally, there may be future technological applications, such as “reading” and “writing” information into Rydberg atoms in the form of subharmonic resonances.

1 Introduction

The present article builds on work first discussed in [1]; related work can be found in [2],[3],[4],[5],[6]. The Rydberg atom is considered here, with the key example being of a hydrogen atom in a high excited state. This research is intended both to provide possible interesting technological innovations, but perhaps more importantly to advance the theory of stochastic electrodynamics (SED). We will assume in this article that the quantum energy number of the

highly excited outer electron is sufficiently large that the energy changes are essentially continuous; as prescribed by the Bohr's correspondence principle, this means that the excited electron behavior can be treated fairly accurately by classical Newtonian physics. With this restriction, but with also the realization that this condition still describes a huge portion of our universe, namely, many aspects of the plasma state, we will proceed to analyze some previously not recognized nor understood states and behaviors of these atoms. Specifically, we will uncover some semi-stable properties of such atoms, namely, subharmonic resonance states. Some experimental evidence for related states has already been found, which certainly helps compel the analysis here [7]. Knowledge of such changes should be helpful in terms of controlling the excited electron's energy state. One can envision schemes by which controlling the outer electron's state could result in "reading" or "writing" information to an excited atom or group of atoms, likely in a statistical sense, even though the quantized energy states form a near continuum. Other interesting inventive issues to contemplate involve controlling a plasma in novel ways, or perhaps imposing new properties and capabilities for systems such as plasma etching. Moreover, paths to ionization have subtleties not fully investigated before that may prove useful for such pursuits.

As mentioned, this research has two main thrusts. First, there is the "practical" side in that the theoretical predictions of long semi-stable states in hydrogen and Rydberg atoms should be quite testable and should allow new technological innovations in the future. Second, on a much more fundamental side, the work has bearing on the relation between the foundations of quantum mechanics (QM) and a potentially more fundamental understanding of such phenomena. In particular, we are referring here to the theory of SED, which was advanced in the 1960s by Marshall and Boyer [8], [9], [10]. SED has been seriously proposed as a deeper basis for QM, particularly regarding atomic physics. It consists of classical electrodynamics, but with the consideration that thermodynamic equilibrium situations of classical charged particles must necessarily be in equilibrium with classical electromagnetic radiation, since accelerations and decelerations of charged particles create electromagnetic radiation. In turn, electromagnetic radiation influences the motion of charged particles. Marshall's and Boyer's separate work both came to the conclusion that for thermodynamic equilibrium to occur between classical charged particles and classical electromagnetic radiation, it was essential that nonzero electromagnetic radiation exists at temperature $T = 0$, as well as for $T > 0$. At $T = 0$, these researchers showed that the radiation spectrum must be Lorentz invariant, which led to a derivation of the spectral form of "classical electromagnetic zero-point (ZP) radiation" [11],[12]. Many other properties were later discovered, including a derivation that this is the only nonzero spectrum that satisfies the thermodynamic definition of absolute $T = 0$, where no heat can flow during a reversible isothermal thermodynamic operation [13]. Boyer's and Marshall's work also led to classical physics derivations of the proper spectral form for $T > 0$, namely, the Planck spectrum plus ZP radiation.

This theory of SED continued to be pursued by both Boyer and Marshall, as

well as a number of other researchers, into the early 1990s and beyond [8],[9],[10]. SED investigations have shown, without qualification, that treating classical electromagnetic radiation and charged particles consistently as a natural interacting system, greatly expands the ability of classical physics to accurately predict phenomena around us. In several cases, it has offered faster and more physically intuitive calculational means than conventional QM, while still agreeing with QM predictions. Several key examples are: (1) systems of linear electric dipole for modeling various behaviors of atoms [8],[9],[10], (2) uniformly accelerating a system of electric dipole harmonic oscillators through the vacuum [14], [15], [16], [17] and (3) Casimir and full retarded van der Waals force calculations at different temperature values and all distances [18], [19], [13], [20], [21], and (4) diamagnetic effects [22], [23]. A key aspect of this theory is that \hbar naturally arises as the scale factor of homogeneous, random, classical electromagnetic radiation at $T = 0$.

Of particular relevance to the present article, was a significant insight by Boyer in 1975 [24], where he suggested that ZP radiation might provide the stochastic mechanism to prevent the collapse of a classical hydrogen atom. His suggestion was backed up by approximate calculations involving energy radiated versus work done by incident radiation on the rapidly moving classical electron. Of course, atomic collapse is precisely the problem that confronted Rutherford upon the discovery of the nucleus and his subsequent model of the atom in 1911. Indeed, we now know that the collapse of Rutherford's classical hydrogen atom, due to radiated energy, should occur within about 10^{-11} s [2]. This problem of collapse motivated Bohr to introduce his energy quantization feature into his 1913 atomic model, that eventually led to even more profound QM directions in the 1920s by Heisenberg, Schrödinger, Dirac, etc.

In SED, carrying out the full hydrogen analysis in an analytic form has proven intractable to date, as there are nonlinear stochastic differential equations involved and an infinite spectrum of driving frequencies acting. Consequently, in 2003 this problem was placed on a computer [6] to calculate whether Boyer's idea might really hold in detail for hydrogen. The results looked very promising, as the ground state of hydrogen was indeed predicted for the equilibrium probability distribution. However, as described in this same article [6], calculational approximations were made to reduce the computational burden, thereby making the problem more computationally tractable at the time in the early 2000s.

In recent years, Nieuwenhuizen and Liska [25], [26], [27] have probed on these simulations much deeper, using far more computational power and less approximations, although certainly approximations still were needed to obtain tractable results. They found that for shorter times of tracking the electron trajectories, the trend was seen toward the ground state that was obtained in [6], but upon proceeding to much longer times, these results changed, with eventual "ionization" of the electron occurring.

Still, it must be mentioned that despite the in-depth work in [25], [26], [27], a concern naturally arises on the very nontrivial problem of simulating an inherently chaotic system due to a nonlinear binding potential, while acted upon

by a rapidly changing and essentially infinite force (ZP radiation) with an infinite frequency spectrum. Upon changing (either improving or lessening) the numerical accuracy of the simulation even slightly, every trajectory in the simulation will be changed enormously due to the inherently mathematical chaotic nature of the problem. The problem is exasperated the farther out in time one carries the simulation. In addition, approximations such as the moving window of frequencies that were employed in all these simulations [6], [25], [26], and the chosen relativistic approximations in [26], provide some concern on how to close the discussion. Despite considerable analysis carried out, the complicated computational nature of this nonlinear, chaotic and stochastic problem with an infinite spectrum of driving frequencies, still raises questions. Indeed, the difficulties seem analogous in ways to the infinities that plagued QED, until finding some resolution due to the important work by physicists like Feynman and Schwinger.

Nevertheless, it is most interesting that classical “atomic collapse” due to orbital acceleration radiating energy away, is essentially not the problem any longer! Instead, the main problem is that the classical electron eventually wanders off (*i.e.*, appears to “ionize”) from the proton that binds it by the Coulombic potential $-\frac{e^2}{r}$ [28]. Thus, clearly the classical electromagnetic ZP field has a very profound effect on the classical hydrogen problem, completely changing the expectation of collapse by physicists like Rutherford and Bohr. As has often been said in “SED circles”, if physicists like Planck and Bohr had thought of consistently treating classical electromagnetic radiation and classical charged particles interactions, they might not have made the QM assumptions that they did, particularly in the case of Planck, who was loath to impose energy quantization constraints on oscillators.

However, there are still other issues of concern. A glaring one to the author is that we do not have a deep understanding, nor much of a qualitative one, for how SED might explain “excited states” and the associated narrow linewidth spectra in atomic physics. “Excited states” have been studied successfully in SED for electric dipole simple harmonic oscillators (SHO), but that is quite different, as emission and absorption occur in a SHO in a narrow band around a sole resonant frequency.

Herein lies a major motivation for the present article. This work was initiated to gain deeper insight about excited states in hydrogen. As we often forget, modern QM still hinges on certain classical notions, such as the classical binding potential for atomic physics that is inserted into Schrödinger’s or Dirac’s equation. The classical physics of SED has yielded considerable agreement with QM predictions, while “simply” pursuing the full inclusion of charged particle motion and electromagnetic radiation. This article examines the physical dynamics of a classical electron orbiting a classical nucleus in more earnest, with classical radiation reaction and an incident circularly polarized (CP) plane wave acting, not just at resonant frequencies, but also at what turns out to be a most interesting behavior, namely, at subharmonic resonant conditions. As will be seen, long semi-stable states can be created. Moreover, “quantized-like”

properties occur, mainly in the eccentricity of the orbit before eventual decay sets in.

Thus, besides providing a testable new phenomena and possible new technological applications, the information gained here may well be helpful in understanding how excited states may arise in SED. Of course the full background radiation would need to be included to push this work further, but one needs to start somewhere, and the fact that extended classical states with unusual properties of long durations and the unique eccentricity properties, can only be helpful in sorting out the needed dynamical understanding.

Reference [1] showed that when a CP plane wave is directed normal to the outer electron's orbit, strong subharmonic resonances occur that prevent orbital decay for many orders of magnitude compared to the classical orbital period, and under a fairly wide range of conditions. As shown, if the electric field amplitude of the CP light exceeds a certain value that depends to first degree on the order of the subharmonic resonance, but also on the semimajor axis value and relative phase, then orbital and energy decay can be held at bay for times long compared to the classical time of orbital decay.

By subharmonic resonance, we mean here the behavior of the classical electron's orbit when the period of the orbit is equal to an integer multiple of $n = 2, 3, 4, 5, \dots$, etc., times the period of the incident CP plane wave; or, in other words, the orbital frequency of the classical electron orbit is equal to $\frac{1}{2}, \frac{1}{3}, \frac{1}{4}$, etc., to that of the frequency of the incident plane wave. Here we will show that when the classical electron is caught in one of these subharmonic resonances, starting initially in a circular orbit, then the semimajor axis, a , remains fairly constant, with a relatively small fluctuation that grows larger and larger over time. Meanwhile, the semiminor axis b steadily decreases, thereby making the orbit more and more elliptical. Consequently, the eccentricity, ε , of the orbit, given by

$$\varepsilon = \sqrt{1 - \left(\frac{b}{a}\right)^2}, \quad (1)$$

steadily increases during this time, starting at zero and increasing toward unity, until a particular critical value, which we will call $\varepsilon_{\text{crit},n}$, is reached. At that moment, the classical electron falls out of subharmonic resonance and the orbit falls into steady decline. As shown here, $\varepsilon_{\text{crit},n}$ is only dependent on the particular subharmonic state, n . Thus, for decay from a near circular orbit, to any subharmonic resonance of state $n = 2$ (incident light's frequency is twice that of the electron's orbital frequency), one obtains the rather surprising result that the subsequent transition from resonance to orbital decay occurs when the eccentricity reaches the value of $\varepsilon_{\text{crit},2} \approx 0.554$. This transition holds for any resonant semimajor axis a value, such as 5 \AA or 50 \AA , that satisfies the classical orbit criteria. Likewise, for $n = 3$, $\varepsilon_{\text{crit},3} \approx 0.671$; for $n = 4$, $\varepsilon_{\text{crit},4} \approx 0.732$. Simulation results will show this behavior, but in addition we will derive why these specific $\varepsilon_{\text{crit},n}$ values occur in Sec. IV, arriving at an analytic expression for them.

Interesting and related experimental work related to the theory and simulation work reported here, has been carried out by others. For example, there appears to be suggestive connections with the experimental work in [7], [29], [30] involving applied microwaves perturbing atomic Rydberg systems. Their work involve both ionization and stabilization effects that depend on many critical factors for Rydberg atoms.

The work in the present article was initiated to provide a deeper insight into the simple classical electron dynamics within a Coulombic potential. As will be seen, without question the dynamical behavior shown here, turns out to be quite rich. However, some of the incentive here was also to investigate whether any classical connection could be made to the excited states of hydrogen in quantum behavior, thereby helping to go beyond the thermodynamic equilibrium state at absolute zero temperature for the “ground state.” This article reveals clear means by which long resonant states can exist in a classical model of hydrogen, plus quantized like behaviors for when resonant states end (*i.e.*, the critical eccentricities discussed earlier).

However, despite the surprising and interesting classical phenomena predicted here, an explanation for excited states in quantum phenomena via SED theory cannot yet be claimed. Still, the phenomena predicted here should indeed hold for real Rydberg atoms. Thus, this work does not, at this point, provide concrete insight into excited states in SED, but it does predict a very real behavior that might be important in future technologies for imposing resonant states on atoms in highly excited states.

A quick way to clarify this discussion on subharmonic resonance is to simply show some simulations of this phenomena, which we turn to next in Sec. II. After these representative simulations, Sec. III turns to the specific equations governing this phenomena and our method for extracting the near elliptical parameters for the orbits. Section IV then analyzes and derives a formula for $\varepsilon_{\text{crit},n}$ for different subharmonic resonances. Concluding comments are in Sec. V, including comments on the emphasis on CP waves and initial circular orbits. Note that additional supportive analysis, simulation plots, and examples for $n = 4, 5, 6$, are contained at [31].

2 Simulation examples

Figures 1 and 2 pertain to a typical example of an $n = 2$ subharmonic resonance situation where the classical electron begins in a circular orbit, in this case with radius 5.162 \AA . The trajectory here is well within the near continuum quantum domain, enabling the motion to be described by the Lorentz-Dirac equation [32],[33], more of which will be said in the subsequent section. In this simulation, the amplitude of the electric field of the CP wave was chosen to be $A = 50 \text{ statvolt/cm}$, in cgs units. The angular frequency of the CP wave, in this simulation, is given by $\omega_1 = \left(\frac{e^2}{ma_1^3}\right)^{1/2}$, where the charge of the classical electron is $e = 4.80298 \times 10^{-10} \text{ esu}$, the mass of the electron is $m = 9.1091 \times 10^{-28} \text{ g}$, and

here a_1 , for this simulation, was chosen to be $3.0 \text{ \AA} = 3.0 \times 10^{-8} \text{ cm}$. Thus, $\omega_1 = 3.0626 \times 10^{15} \text{ s}^{-1}$. The $n = 2$ net angular frequency resonance, when a CP wave is applied with an angular frequency ω_1 , is given by $\omega_2 = \frac{\omega_1}{2}$, which occurs if $\omega_2 = \left(\frac{e^2}{ma_2^3}\right)^{1/2} = \frac{1}{2}\omega_1 = \frac{1}{2}\left(\frac{e^2}{ma_1^3}\right)^{1/2}$, or $a_2 = a_1 \times 2^{2/3}$. For this simulation, that means $a_2 = 3.0 \text{ \AA} \times 2^{2/3} \approx 4.7622 \text{ \AA}$. As can be seen from Fig.1, this is precisely where this resonance takes place, and indeed holds to many decimal places if we were to zoom in on the plot much closer.

Thus, the orbit steadily decreases at first as electromagnetic energy is radiated away due to the orbiting motion, but when the $n = 2$ subharmonic is reached at $a_2 \approx 4.7622 \text{ \AA}$, a strong resonance occurs, at $t \approx 3.5 \times 10^{-9} \text{ s}$. The resonance lasted for about $1.17 \times 10^{-7} \text{ s}$, at which point orbital decay began again. During the resonance the semimajor axis remained fairly constant, although, actually, a small, but increasing oscillation in a occurs, as can be seen by the ‘‘thickening’’ of the a vs. t plot. During this resonance, a total of about 2.8×10^7 classical orbits occurred, clearly a significance resonance.

Figure 1 also shows the eccentricity, ε , versus time (scale on the right axis). Here, $\varepsilon = 0$ at $t = 0$, since the orbit was initially circular. Once the $n = 2$ resonance is reached, then ε immediately begins to increase, as the orbit maintains a fairly constant a , but the overall orbit becomes more and more elliptical as the semimajor axis b decreases. This increase in ε continues until $\varepsilon \approx 0.544$, at which point the orbit falls into decay. As mentioned earlier, this result would still be true if a_2 was chosen much differently, such as 10 \AA or 50 \AA , typical numbers for the excited electron in a Rydberg atom.

Figure 2 focuses in on the point of decay just described, for ε vs. t , at $t \approx 1.17 \times 10^{-7} \text{ s}$. The oscillations in ε can be seen clearly here; if we were to focus in on a vs. t at this point, the same nature of oscillations would be seen. However, more important is the critical eccentricity point at which the eccentricity reaches an average value of $\varepsilon \approx 0.544$, at which point orbital decay sets in. Again, we’ll deduce this value in Sec. IV.

The time in resonance before decay sets in certainly depends on A as well as the initial phase α between the CP wave and the orbit, all very similar to the studies carried out on primary ($n = 1$) resonance in previous studies [4],[5], where the orbital and CP wave period are essentially the same. In addition, the length of time in resonance also depends on the starting point of a above the resonance point, and if the initial orbit is circular or has some degree of ellipticity.

Similar to the $n = 2$ example in Figs. 1 and 2, Figs. 3 and 4 show a subharmonic resonance when $n = 3$, where the incident CP wave has a frequency three times that of the electron’s orbital frequency. The electron’s orbit started in a circular path with $r = 0.7 \text{ \AA}$. To ‘‘catch’’ an electron in an $n = 3$ state, versus an $n = 2$ one, for similar radii values, requires much stronger CP plane wave amplitudes, as discussed in [1] (*e.g.*, see Fig. 4 in [1]). Here, $A = 35,000$ statvolt/cm was used. If A is too low, then the resonance condition is not met, and the electron will continue to decay through the $n = 3$ resonance point. A related important characteristic feature is that the larger A is above the critical

value to “catch and hold” the decaying orbit, the wider the a vs. t resonance envelope becomes as t increases, as will be clearly seen shortly in Fig. 5.

In Fig. 3, the angular frequency of the CP wave was chosen to be $\omega_1 = \left(\frac{e^2}{ma_1^3}\right)^{1/2}$, with $a_1 = 0.3 \text{ \AA}$, so $\omega_1 = 9.6848 \times 10^{16} \text{ s}^{-1}$, while the resonant orbital angular frequency was $\omega_3 = \frac{1}{3}\omega_1$. As seen in Fig. 3, the electron decays from the starting point of $r = 0.7 \text{ \AA}$. During this initial decay period, the electron’s motion is barely effected by the CP wave. Although not shown, if plots with $A = 0$ and $A = 35,000 \text{ statvolt/cm}$, or other values of A , were superimposed, little difference would be seen until resonance is reached. However, when the semimajor axis (which up to now is the same as the radius) decays to the point of $a_3 = a_1 \times 3^{2/3} = 0.6241 \text{ \AA}$, then the CP wave’s action on the orbit becomes very significant. The decaying orbit stops, the semimajor axis a vs. t becomes fairly flat, although with an envelope, due to oscillations in a vs. t , that widens as t increases.

Figure 3 also contains two additional plots not in Fig. 1: the semiminor axis, b vs. t , plus θ_0 vs. t , where $\theta_0(t)$ will be defined more precisely in Sec. III, but is essentially the angle of rotation of the semimajor axis, as a function of time. As shown in Fig. 3, while $a(t)$ remains fairly flat in resonance, albeit for the increase in oscillation about the center value of $a_3 = 0.6241 \text{ \AA}$, $b(t)$ steadily decreases its average value, while also increasing in oscillation about its center value. The decrease in $b(t)$ is what gives rise to the increase in $\varepsilon = \sqrt{1 - \left(\frac{b}{a}\right)^2}$. Until the $n = 3$ resonance point is reached, $\varepsilon \approx 0$. After reaching the resonance point, ε increases steadily until the orbit goes back into a decaying mode, when $\varepsilon \approx 0.669$ (Fig. 4). The value of 0.6706 is shown, which is the analytic value computed in Sec. IV, and close (good to three digits) to the simulated/computed value, although not as close as the $n = 2$ case shown in Sec. I, which agreed to four digits.

As seen in Fig. 3, until resonance is reached, $\theta_0 \approx 0$. After the start of resonance, which occurred at about $t \approx 1.1 \times 10^{-11} \text{ s}$, the orbit becomes more and more elliptical and the axis of the orbit undergoes rotations adding up to about 2800 radians, or about 446 revolutions. Of course during this resonance period the classical electron undergoes orders of magnitude more revolutions about the nucleus, namely, about 6×10^5 revolutions, or about a factor of 1300 for this particular example.

Resonance makes the axis of the orbit rotate, with larger amounts of rotation occurring as A becomes larger. Before and after resonance, however, the axis rotations essentially stop, which makes sense since at these points, the orbit is little influenced by the CP wave and is largely dictated by the $1/r^2$ Coulombic attraction to the nucleus, which of course results in the well known elliptical orbit behavior explained so long ago by Newton.

The plots shown are in sharp contrast to the work shown in Ref. [1], where the analysis concentrated on radius and energy versus time, as opposed to recognizing that the orbits were changing from circular to becoming more elliptical in nature. Consequently, the previous work did not touch on the essentially con-

stant semimajor axis during resonance, nor did it recognize the critical values of ε when orbital subharmonic resonance “broke” and turned back into orbital decay.

Finally, before turning to equations governing this phenomena and providing a deeper physical understanding, Figs. 5 and 6 show general properties that occur at subharmonic resonances. Figures 5 and 6 demonstrates the “universality” of $\varepsilon_{\text{crit},n} \approx 0.554$ for the $n = 2$ subharmonic resonance, for the situation where the classical electron’s orbit begins in a circular orbit with semimajor axis a greater than the $a_2 = a_1 2^{2/3}$ resonance point, and with the CP wave amplitude large enough to cause resonance once the orbit decays to a_2 . Both figures concern the situation where $a_1 = 0.5 \text{ \AA}$, or the angular frequency of the CP wave is $\omega_1 = \left(\frac{e^2}{ma_1^3}\right)^{1/2} = 4.5011 \times 10^{16} \text{ s}^{-1}$. The starting radius is 0.9 \AA , and six simulations are superimposed, each with a different CP wave amplitude: $A = 100, 500, 1000, 5000, 10,000, \text{ and } 50,000 \text{ statvolt/cm}$.

In Fig. 5, a vs. t is shown. The electron is “caught” at $a_2 = a_1 2^{2/3} = 0.7937 \text{ \AA}$ in all six cases. The length of time in the $n = 2$ subharmonic resonance varies, with the 500 statvolt/cm being the longest, then with decreasing times in the order of 1000, 5000, 10,000, 50,000, and 100 statvolt/cm. Similar situations were shown for the $n = 1$ case in Refs. [4] and [5]. The larger the value of A , the larger becomes the “envelope” of the a vs. t fluctuations around the $a_2 = 0.7937 \text{ \AA}$ point, with the widest ending envelope here being the one with $A = 50,000 \text{ statvolt/cm}$.

Figure 6 turns to examine these same simulations, but now plotting $\varepsilon(t)$ vs. t . In each case, ε starts at zero, since the initial orbit is circular, then increases until the value of $\varepsilon_{\text{crit},2} \approx 0.554$, at which point the orbit goes back into decay. The key point is that all have essentially the same value of $\varepsilon_{\text{crit},2}$ for when the orbit changes from one of $n = 2$ subharmonic resonance to orbital decay.

The same type of behavior occurs for increasing values of a_1 , as well as for different subharmonic n states. Specifically: (1) the final eccentricity before decay is very close to 0.554 for $n = 2$, if not even closer to the 0.5542 analytical value later calculated in Sec. IV, with different $\varepsilon_{\text{crit},n}$ values for different n state subharmonic resonances; (2) the envelope around the a vs. t curve always increases in width as A increases; and (3) the length of time of an n resonance certainly depends on the value of A , reaching a longest value (here it was for 500 statvolt/cm), then decreasing as A becomes larger beyond that point.

Incidentally, it is a curious point from a classical physics point of view, that circular orbits have a bit of “preference,” or likelihood of occurrence, over orbits with $\varepsilon > 0$, for simple situations with either no radiation applied, or perhaps one CP wave applied. When a large range of radiation frequencies and amplitudes are applied, as in the stochastic situation of Ref. [6], then the following comment does not hold, but for simple situations as just mentioned, the radiation reaction term in the Lorentz-Dirac equation acts in such a way as to return an initially decaying elliptical orbit back toward a circular (decaying) orbit. This was noted in Ref. [3], Fig. 4, in particular, and also in several points and figures later in [3] where various applied radiation conditions occurred. Here, we also see this

point in Fig. 6, where once the electron falls out of resonance, the radiation reaction term acts to make $\varepsilon \rightarrow 0$ as the orbit decays.

3 Equations of motion and elliptical parameter extraction

The motion of the classical electron, with point charge $-e$ and mass m , no spin, and for nonrelativistic speeds, while bound to an infinitely massive center with opposite point charge $+e$ (nucleus), is described by the nonrelativistic Lorentz-Dirac (LD) equation of motion in cgs units: [32],[34]:

$$m \frac{d^2 \tilde{\mathbf{z}}}{dt^2} = -e^2 \frac{\tilde{\mathbf{z}}}{|\tilde{\mathbf{z}}|^3} + \frac{2e^2}{3c^3} \frac{d^3 \tilde{\mathbf{z}}}{dt^3} - e \mathbf{E}_{\text{CP}}[\mathbf{z}(t), t] - \frac{e}{c} \frac{d\tilde{\mathbf{z}}}{dt} \times \mathbf{B}_{\text{CP}}[\mathbf{z}(t), t] \quad . \quad (2)$$

Here, m is the mass of the classical electron, $-e$ is its charge, c is the speed of light, $-e^2 \frac{\tilde{\mathbf{z}}}{|\tilde{\mathbf{z}}|^3}$ is the Coulombic binding force, $-\frac{2e^2}{3c^3} \frac{d^3 \tilde{\mathbf{z}}}{dt^3}$ is the nonrelativistic radiation reaction term, and $\mathbf{E}[\mathbf{z}(t), t]$ and $\mathbf{B}[\mathbf{z}(t), t]$ are additional electric and magnetic fields acting on the system, acting via the Lorentz force on the motion of the particle. Certainly other radiation fields than a CP wave can be examined, but this study concentrates only on the effects of a CP wave. Section V comments further on this emphasis, with qualitative discussions on other choices.

In place of (2), the full relativistic LD equation [32] can certainly be used, but for typical Rydberg orbits, where the orbit radius is quite large, it is quite unnecessary as the classical electron's speed $|\mathbf{v}|$ is so small compared to the speed of light. For circular orbits, only when the radius r shrinks to about 0.28 \AA is $v/c \approx 0.01$, or 1%, and not until r is nearly 100 times smaller than that does v/c reach about 0.1, or 10%, where relativistic corrections are then clearly needed. For elliptical orbits, the need for relativistic corrects can occur earlier, as the maximum speed in an elliptical orbit from the nonrelativistic and the classical Kepler-like equation of

$$m \frac{d^2 \tilde{\mathbf{z}}}{dt^2} = -e^2 \frac{\tilde{\mathbf{z}}}{|\tilde{\mathbf{z}}|^3} \quad , \quad (3)$$

is given by

$$v_{\text{max}} = \frac{e}{m^{1/2} a^{1/2}} \left(\frac{1 + \varepsilon}{1 - \varepsilon} \right)^{1/2} \quad . \quad (4)$$

When $\varepsilon = 0$, the orbit is circular, $v_{\text{max}}/c = \frac{e}{(ma)^{1/2} c}$, and it is this quantity that equals 0.01 when $a \approx 0.28 \text{ \AA}$, as mentioned before. However, as can be seen from (4), for extremely elliptical orbits, where ε approaches 1, then the full relativistic LD equations should be used. We will not be examining such situations here, nor examining very small a situations.

The “damping” term in (2) of $\frac{2e^2}{3c^3} \frac{d^3 \mathbf{z}}{dt^3}$ is much weaker than other forces, due to the extremely small magnitude of

$$\tau \equiv \frac{2e^2}{3c^3} = 6.266031 \times 10^{-24} \text{ s} . \quad (5)$$

Moreover, the magnitude of the Lorentz force of the CP plane wave acting on the electron, is typically orders of magnitude smaller than the Coulombic force of the nucleus, $-e^2 \frac{\mathbf{z}}{|\mathbf{z}|^3}$, acting on the electron, at least for the simulation examples considered here, as well as what might normally be encountered experimentally. Hence, as is often done in such problems, the small term $\frac{2e^2}{3c^3} \frac{d^3 \mathbf{z}}{dt^3}$ is approximated by [32],[34]:

$$\begin{aligned} \frac{2e^2}{3c^3} \frac{d^3 \mathbf{z}}{dt^3} &= \frac{2e^2}{3c^3} \frac{d}{dt} \left(\frac{d^2 \mathbf{z}}{dt^2} \right) \approx \frac{2e^2}{3c^3} \frac{d}{dt} \left(-e^2 \frac{\mathbf{z}}{|\mathbf{z}|^3} \right) \\ &= -\frac{2e^4}{3c^3} \left[\frac{\frac{d\mathbf{z}}{dt}}{|\mathbf{z}|^3} - \frac{3\mathbf{z}(\mathbf{z} \cdot \frac{d\mathbf{z}}{dt})}{|\mathbf{z}|^5} \right] . \end{aligned} \quad (6)$$

The situation considered here is where the orbit of the classical electron begins in the $x - y$ plane and where the CP plane wave is directed in the $-\hat{\mathbf{z}}$ direction toward the $z = 0$, $x - y$ plane. The following expressions for the CP electric and magnetic fields are due to two traveling plane waves, one $\frac{\pi}{2}$ with respect to the phase of the other, but both traveling in the $-\hat{\mathbf{z}}$ direction, so $\mathbf{k} = -\hat{\mathbf{z}} \frac{\omega_1}{c}$, where ω_1 is the angular frequency of the incident plane waves. Thus,

$$\hat{\mathbf{k}} = -\hat{\mathbf{z}} = \frac{\tilde{\mathbf{E}}_{\text{CP}} \times \tilde{\mathbf{B}}_{\text{CP}}}{|\tilde{\mathbf{E}}_{\text{CP}} \times \tilde{\mathbf{B}}_{\text{CP}}|} , \quad (7)$$

and

$$\tilde{\mathbf{E}}_{\text{CP}} = A \left[\hat{\mathbf{x}} \cos \left(\tilde{\mathbf{k}} \cdot \tilde{\mathbf{z}} - \omega_1 t + \frac{\pi}{2} - \alpha \right) - \hat{\mathbf{y}} \cos \left(\tilde{\mathbf{k}} \cdot \tilde{\mathbf{z}} - \omega_1 t - \alpha \right) \right] , \quad (8)$$

$$\tilde{\mathbf{B}}_{\text{CP}} = A \left[-\hat{\mathbf{x}} \cos \left(\tilde{\mathbf{k}} \cdot \tilde{\mathbf{z}} - \omega_1 t - \alpha \right) - \hat{\mathbf{y}} \cos \left(\tilde{\mathbf{k}} \cdot \tilde{\mathbf{z}} - \omega_1 t + \frac{\pi}{2} - \alpha \right) \right] . \quad (9)$$

The electric and magnetic fields lie solely in the $x - y$ plane of the orbiting electron, with $\hat{\mathbf{k}} \times \tilde{\mathbf{E}}_{\text{CP}} = -\hat{\mathbf{z}} \times \tilde{\mathbf{E}}_{\text{CP}} = \tilde{\mathbf{B}}_{\text{CP}}$. The electric field vector points and rotates in the counterclockwise direction, with a constant magnitude of A , with the same for the magnetic field, which is perpendicular to the electric field. The phase factor α allows for the situation where the force $-e\tilde{\mathbf{E}}_{\text{CP}}$ and the velocity of the electron, $\frac{d\tilde{\mathbf{z}}}{dt}$, are at an angle α at $t = 0$. The significant effect of α on length of time to decay was explored in some detail in Ref. [5] for the primary resonance case of $n = 1$; the effect can be quite significant. Section V comments briefly on the interest here for a single CP wave; however, clearly the infinite other types of possible radiation states, simply magnify the phenomena that might occur.

The only force that acts to move the classical electron out of the $x - y$ plane orbit is due to the Lorentz force from the magnetic field, or

$$-\frac{e}{c} \frac{d\tilde{\mathbf{z}}}{dt} \times \tilde{\mathbf{B}}_{\text{CP}} [\tilde{\mathbf{z}}(t), t] \quad .$$

The magnitude of this force is typically fairly weak force due to the $1/c$ factor. For the length of time of the simulations considered here, the contribution of this force in the z direction, is fairly negligible. It acts to slowly change the planar orbit to a more 3D behavior, but the time scale is quite long.

Consequently, our following analysis will entail the CP fields in the $x - y$ plane at $z = 0$. Rewriting slightly:

$$\mathbf{E}_{\text{CP}} = A \left[\hat{\mathbf{x}} \cos \left(\omega_1 t - \frac{\pi}{2} + \alpha \right) - \hat{\mathbf{y}} \cos (\omega_1 t + \alpha) \right] \quad , \quad (10)$$

$$\tilde{\mathbf{B}}_{\text{CP}} = A \left[-\hat{\mathbf{x}} \cos (\omega_1 t + \alpha) - \hat{\mathbf{y}} \cos \left(\omega_1 t - \frac{\pi}{2} + \alpha \right) \right] \quad . \quad (11)$$

Combining (2) with (6), (10) and (11), and writing the equations of motion in the $x - y$ plane using polar coordinates, r and θ , results in:

$$m \left(\ddot{r} - r\dot{\theta}^2 \right) = -\frac{e^2}{r^2} + 2\tau e^2 \frac{\dot{r}}{r^3} + eA \sin (\theta - \omega_1 t - \alpha) \quad , \quad (12)$$

and

$$m \left(r\ddot{\theta} + 2\dot{r}\dot{\theta} \right) = -\tau e^2 \frac{\dot{\theta}}{r^2} + eA \cos (\theta - \omega_1 t - \alpha) \quad . \quad (13)$$

The left side of (12) equals the mass times the acceleration in the positive radial direction; the right side equals the sum of forces in the same direction. The left side of (13) equals the mass times the acceleration in the increasing θ direction; the right side equals the sum of forces in the same direction.

The nonlinear, coupled, ordinary differential equations (12) and (13), second order in time, will be solved numerically here using an adaptive stepsize Bulirsch-Stoer routine [35], similar to the work in [1]. However, here a least squares method was developed and implemented to extract elliptical parameters matching the electron's slowly changing orbit. The premise here is that with the Coulombic potential being the dominant forcing mechanism on the orbit, then the orbit should be essentially elliptical, since via Newton, (3) leads to elliptical orbits for bound systems. The CP plane wave is the next strongest force, which can result in the elliptical orbit slowly changing, while the damping term acts to slowly shrink the orbit. Indeed, if no CP wave is present, the damping term slowly collapses any elliptical orbit, making it more circular, and shrinking the radius to zero (for example, see Fig. 4 in [3], where this effect is clearly shown). Of course, when the radius becomes too small, perhaps less than about 0.1 \AA ($v_{\text{max}}/c \approx 0.017$), then the relativistic Lorentz-Dirac equation should be used.

Thus, $r(t)$ and $\theta(t)$ were numerically solved for here, plus a parameter extraction method was implemented to approximate the trajectory as an ellipse

that slowly rotates and changes in the size of its two axes. The parameters extracted were the approximate values for the semimajor axis, a , the eccentricity, ε , and the angle, θ_0 , of the center axis of the ellipse with respect to the x axis. From a and ε , one can obtain the semiminor axis, b , from (1). The radius of the orbit, from the nucleus center of the Coulombic force (again, approximating that this much more massive center does not move), can be written as a function of θ via

$$r(\theta) = \frac{a(1 - \varepsilon^2)}{1 - \varepsilon \cos(\theta - \theta_0)} \quad , \quad (14)$$

where $x = r \cos(\theta)$ and $y = r \sin(\theta)$. The above expression, when a , ε , θ_0 are constants, is the geometrical solution to the Kepler-Coulombic (3) equation. The parameters a , ε , and θ_0 were obtained via the least squares method described in [3], that keeps track of r and θ values of the orbiting particle, for N points, where N is made large enough to encompass at least one or more orbits. Thus, a , ε , and θ_0 were treated as slowly changing parameters in time to match the approximate elliptical orbit at any instant. These parameters were extracted by rewriting (14) as

$$\frac{1}{r} = \frac{1}{a(1 - \varepsilon^2)} - \left[\frac{\varepsilon \cos(\theta_0)}{a(1 - \varepsilon^2)} \right] \cos(\theta) - \left[\frac{\varepsilon \sin(\theta_0)}{a(1 - \varepsilon^2)} \right] \sin(\theta) \quad , \quad (15)$$

and then making a table of $1/r$, $\cos(\theta)$, and $\sin(\theta)$ for N points, sequentially in time. The parameters

$$P_1 \equiv \frac{1}{a(1 - \varepsilon^2)} \quad , \quad (16)$$

$$P_2 \equiv -\frac{\varepsilon \cos(\theta_0)}{a(1 - \varepsilon^2)} \quad , \quad (17)$$

$$P_3 \equiv -\frac{\varepsilon \sin(\theta_0)}{a(1 - \varepsilon^2)} \quad , \quad (18)$$

were then obtained by least-squares methods. From P_1 , P_2 , and P_3 , then a , ε , and θ_0 were obtained.

4 Analysis of critical values of ε

To deduce the values of $\varepsilon_{\text{crit},n}$, we will start with the conserved quantities in the classic Kepler-Coulombic case of a central force with a $1/r^2$ dependence, which in our case means the situation where no CP plane wave acts and no radiation reaction exists. We will then examine how these otherwise conserved quantities, change with time due to the CP wave and the radiation reaction. The natural conservation quantities to consider are the energy, the angular momentum vector, and the Laplace-Runge-Lenz vector. As discussed in [36], the angular momentum vector and the energy alone contain only four independent constants of the motion, while the Laplace-Runge-Lenz vector adds one more. We will make use of this work, nicely presented in texts such as [36] and [37]. We make

the approximation that the orbit remains essentially in a two dimensional plane during the duration of the resonance and the subsequent decay and that the natural Coulombic based orbit is slowly modified by the additional forces of the CP plane wave and the small, but constant, radiation reaction. Identifying the normally constant Coulombic parameters and having them slowly change due to these additional forces, will be sufficient to deduce much about $\varepsilon_{\text{crit},n}$.

Multiplying (12) by the radial speed \dot{r} , and multiplying (13) by the speed $r\dot{\theta}$ in the increasing θ direction, adding the two contributions, then yields, after a bit of manipulation:

$$\begin{aligned} & \frac{d}{dt} \left[\frac{m}{2} \left(\dot{r}^2 + r^2 \dot{\theta}^2 \right) - \frac{e^2}{r} \right] \\ &= \tau e^2 \left(2 \frac{\dot{r}^2}{r^3} - \frac{\dot{\theta}^2}{r} \right) + eA \left[\dot{r} \sin(\theta - \omega_1 t - \alpha) + r \dot{\theta} \cos(\theta - \omega_1 t - \alpha) \right] . \end{aligned} \quad (19)$$

The left side is the time rate of change of the kinetic energy, in polar coordinates, plus the time rate of change of the Coulombic potential energy. On the right side, the first term is the nonrelativistic rate of work by the radiation reaction term, very weak, but always present and causing the tendency for orbital decay. The second term on the right is the rate of work by the Lorentz force of the CP wave acting on the classical electron, normally varying rapidly in sign, but with a sign correlation occurring when orbital angular frequency and applied frequency ω_1 match up. If the radiation reaction and CP wave did not exist, then the left side would equal zero, and the kinetic plus Coulombic potential energy would be a constant.

Similarly, the angular momentum rate equation can be deduced by multiplying (13) by r and converting it into:

$$\frac{d}{dt} \left(mr^2 \dot{\theta} \right) = -\frac{\tau e^2 \dot{\theta}}{r} + erA \cos(\theta - \omega_1 t - \alpha) . \quad (20)$$

The left side is the time rate of change of $L_z = mr^2 \dot{\theta}$, the angular momentum component perpendicular to the plane of the orbit, written in polar coordinates. On the right side, the first term is the nonrelativistic torque expression due to the radiation reaction, again, very weak, but always present. The second term on the right is the torque acting on the orbiting classical electron due to the Lorentz force of the CP wave. If the radiation reaction and CP wave were not present, L_z would be a constant.

Following standard treatments such as in [36], [37], [38], when the right sides of (19) and (20) equal zero, corresponding to the pure Kepler-Coulombic problem of (3), then for a bound orbit,

$$\dot{\theta} = \frac{e[1 - \varepsilon \cos(\theta - \theta_0)]^2}{m^{1/2} a^{3/2} (1 - \varepsilon^2)^{3/2}} , \quad (21)$$

and from (14) and (21)

$$L_z = mr^2 \dot{\theta} \approx e(am)^{1/2} (1 - \varepsilon^2)^{1/2} , \quad (22)$$

where the approximation sign would be replaced by an equality sign if radiation damping and the CP wave were not present.

Assuming the rate of time variation in a , ε , and θ_0 is small, compared to the much more rapid time variation in $\theta(t)$, then also from (14) and (21), one can show that

$$\frac{m}{2} \left(\dot{r}^2 + r^2 \dot{\theta}^2 \right) - \frac{e^2}{r} \approx -\frac{e^2}{2a} . \quad (23)$$

From (19) and (23),

$$\begin{aligned} \frac{d}{dt} \left(-\frac{e^2}{2a} \right) &\approx \tau e^2 \left(2 \frac{\dot{r}^2}{r^3} - \frac{\dot{\theta}^2}{r} \right) \\ &+ eA \left[\dot{r} \sin(\theta - \omega_1 t - \alpha) + r \dot{\theta} \cos(\theta - \omega_1 t - \alpha) \right] , \end{aligned} \quad (24)$$

and from (20) and (22),

$$\frac{d}{dt} \left[e(am)^{1/2} (1 - \varepsilon^2)^{1/2} \right] \approx -\frac{\tau e^2 \dot{\theta}}{r} + e r A \cos(\theta - \omega_1 t - \alpha) . \quad (25)$$

The simulations reported in this article arise from numerically solving for $r(t)$ and $\theta(t)$ in (12) and (13), while the fitted parameters a , ε , and θ_0 to these orbits come from the least squares fit method discussed in Sec. III. Equations (24) and (25) contain a mixture of these variables and were deduced to enable an understanding of the interesting values of $\varepsilon_{\text{crit},n}$ that result when orbits in a subharmonic state eventually fall out of resonance and turn back into decaying orbital paths.

To ensure that the approximations make sense, [31] offers some insight into the approximations by making direct comparisons between (1) $E = \frac{1}{2} m \tilde{\mathbf{v}}^2 - \frac{e^3}{r}$ and the approximate value of $-\frac{e^2}{2a}$, and (2) $L_z = m r^2 \dot{\theta}$ versus the approximate value of $e(am)^{1/2} (1 - \varepsilon^2)^{1/2}$. For the range of examples covered here and in [31], these two approximations are excellent ones.

To make further progress on deducing the $\varepsilon_{\text{crit},n}$ values, we first note that when in resonance, $a \approx \text{constant}$; hence, the kinetic plus potential energy (23), which is approximately $-\frac{e^2}{2a}$, is therefore also approximately constant. Now, this isn't exactly true, as a is certainly fluctuating when in resonance, and the fluctuation grows over time, as evident from Fig. 5; this fact we will need to take into account. This will be done by taking a short time average,

$$\langle \dots \rangle \equiv \frac{1}{\tau} \int_t^{t+\tau} (\dots) dt' , \quad (26)$$

where the interval τ is sufficiently large to contain many oscillations of the quantities of interest, as in Figs. 2 and 4, but not so large as to miss the key features, such as the start and end of resonance; i.e., we anticipate hundreds or more orbits in time τ , then some of these difficulties can be avoided, and

thereby pertain closer to the idea of a , ε , and θ_0 in the first place, since these parameters are intended to model the relatively slow evolution of the orbit.

By taking this time average over both sides in (24) during resonance, the left side of (24) reduces to essentially zero. Physically, this is equivalent to saying that the time average of the first term on the right, which is negative, and in classical physics is due to electromagnetic energy being radiated off, but is compensated by the positive energy, on average, that is pumped back into the orbit by the CP wave (second term on right side).

Taking a similar time average for (25) also helps. However, the left side does not always equal zero when in resonance, as can be seen by the more detailed work in [31]. The orbit becomes more and more elliptical throughout the evolution of the subharmonic resonance, so ε increases on average, with small oscillations superimposed. When ε reaches its maximum, as in Figs. 1 and 3, then the time rate of change of $\langle \varepsilon \rangle$ is essentially zero. This is the point we are interested in, as this involves the value of $\varepsilon_{\text{crit},n}$.

Physically speaking, the time average of the first term on the right in 25 provides a fairly constant acting torque that decreases the orbital angular momentum. The time average of the second term on the right averages over a stronger, but rapidly varying torque, between positive and negative values, from the CP wave. $\langle L_z \rangle$ decreases while in resonance [31], until orbital decay again sets in. At this point, the CP wave is no longer able to continue to stay in phase on average, particularly in terms of providing a positive average energy to counteract the small but constant radiation reaction. At this point $\langle L_z \rangle$ flattens out, which is where decay sets in, and is where $\langle \frac{d}{dt} L_z \rangle \approx 0$.

The material in [31] has additional information on this last point, showing that a_{initial} needs to be slightly larger than a_n , otherwise $\langle \frac{d}{dt} L_z \rangle$ does not have sufficient time to relax to zero. For example, if a_{initial} is chosen to be right at a_n at the start of the simulation, then although subharmonic resonance may be initiated, $\langle \frac{d}{dt} L_z \rangle$ will not be zero at the end of subharmonic resonance. The result will end in our prediction of $\varepsilon_{\text{crit},n}$ to be correct to only about two digits of accuracy, rather than, for example, the four digits in Fig. 2.

Otherwise, by taking the time average of (24) and (25), setting the left sides to zero near the onset of orbital decay, and taking the ratio of the resulting nonzero terms, we obtain:

$$\frac{\left\langle \frac{\tau e^2 \dot{\theta}}{r} \right\rangle}{\left\langle \tau \frac{e^2}{r^3} \left[2\dot{r}^2 - (r\dot{\theta})^2 \right] \right\rangle} \approx - \frac{\langle e r A \cos(\theta - \omega_1 t - \alpha) \rangle}{\left\langle e A \left[\dot{r} \sin(\theta - \omega_1 t - \alpha) + r \dot{\theta} \cos(\theta - \omega_1 t - \alpha) \right] \right\rangle} . \quad (27)$$

An immediate satisfactory feature of this expression for deducing $\varepsilon_{\text{crit},n}$, is that A cancels out on the right, as expected from Fig. 6. Also, the τe^2 term cancels on the left, and e cancels on the right.

In the denominator on the right,

$$\begin{aligned} & \dot{r} \sin(\theta - \omega_1 t - \alpha) + r \dot{\theta} \cos(\theta - \omega_1 t - \alpha) \\ &= \frac{d}{dt} [r \sin(\theta - \omega_1 t - \alpha)] + r \omega_1 \cos(\theta - \omega_1 t - \alpha) \end{aligned} \quad (28)$$

Upon taking the time average,

$$\begin{aligned} & \left\langle \frac{d}{dt} [r \sin(\theta - \omega_1 t - \alpha)] \right\rangle \\ &= \frac{1}{\tau} \int_t^{t+\tau} \frac{d}{dt'} [r \sin(\theta - \omega_1 t' - \alpha)] dt' \\ &= \frac{1}{\tau} \{r(t+\tau) \sin[\theta(t+\tau) - \omega_1(t+\tau) - \alpha] - r(t) \sin[\theta(t) - \omega_1 t - \alpha]\} . \end{aligned} \quad (29)$$

Since r is bounded, then for a value of τ that is much larger than the period of an orbit, and encompasses a number of the fluctuations in a and ε (examples are shown in [31]), then (29) becomes negligible compared to the time average of the remaining term on the right in (28). Hence,

$$\left\langle \dot{r} \sin(\theta - \omega_1 t - \alpha) + r \dot{\theta} \cos(\theta - \omega_1 t - \alpha) \right\rangle \approx \omega_1 \langle r \cos(\theta - \omega_1 t - \alpha) \rangle , \quad (30)$$

and the right side of (27) then simplifies enormously to simply being $-\frac{1}{\omega_1}$.

Working on the left side of (27) now,

$$\begin{aligned} \left\langle \frac{\dot{\theta}}{r} \right\rangle &= \frac{1}{\tau} \int_t^{t+\tau} dt' \frac{d\theta}{dt'} \frac{1}{r} = \frac{1}{\tau} \int_{\theta(t)}^{\theta(t+\tau)} \frac{d\theta}{r} \\ &= \frac{1}{\tau} \int_{\theta(t)}^{\theta(t+\tau)} \frac{[1 - \varepsilon \cos(\theta - \theta_0)]}{a(1 - \varepsilon^2)} d\theta . \end{aligned} \quad (31)$$

As shown in the simulation figures, a and ε do have a small fluctuation about their center value when in resonance, but if we take their center values along the curves, and recognize the true source of rapid fluctuations, namely $\cos(\theta - \theta_0)$, which fluctuates with every orbit, while a , ε , and θ_0 vary over tens to hundreds of orbits, and if τ is made equal to $N \times T$, where T is the orbital period and N is of the order of perhaps 100, then the second term in the numerator contributes negligibly with larger N . The first term, however, without the large fluctuation on every orbit, can be evaluated via,

$$\frac{1}{\tau} [\theta(t+\tau) - \theta(t)] \approx \frac{1}{(N \times T)} 2\pi N = \frac{2\pi}{T} , \quad (32)$$

which does not diminish as N grows, resulting in the reasonable approximation of

$$\left\langle \frac{\dot{\theta}}{r} \right\rangle \approx \frac{2\pi}{Ta(1-\varepsilon^2)} . \quad (33)$$

Here, a and ε are the central values over which the short time interval during which the average of $\frac{\dot{\theta}}{r}$ was taken, and T is the period of the orbit.

Finally for the denominator on the left in (27), first we note that

$$\dot{r} \approx \dot{\theta} \frac{d}{d\theta} \left[\frac{a(1-\varepsilon^2)}{1-\varepsilon \cos(\theta-\theta_0)} \right] = -\frac{e\varepsilon \sin(\theta-\theta_0)}{m^{1/2}a^{1/2}(1-\varepsilon^2)^{1/2}} , \quad (34)$$

ignoring the small fluctuations in a , ε , and θ_0 here and using (21). Then,

$$\begin{aligned} & \left\langle \frac{2\dot{r}^2 - (r\dot{\theta})^2}{r^3} \right\rangle \\ &= \frac{1}{\tau} \int_{\theta(t)}^{\theta(t+\tau)} \frac{d\theta}{\dot{\theta}} \frac{[2\dot{r}^2 - (r\dot{\theta})^2]}{r^3} \\ &\approx \frac{1}{\tau} \int_{\theta(t)}^{\theta(t+\tau)} \frac{d\theta}{\left\{ \frac{e[1-\varepsilon \cos(\theta-\theta_0)]^2}{m^{1/2}a^{3/2}(1-\varepsilon^2)^{3/2}} \right\} \left[\frac{a(1-\varepsilon^2)}{1-\varepsilon \cos(\theta-\theta_0)} \right]^3} \left\{ 2 \left[-\frac{e\varepsilon \sin(\theta-\theta_0)}{m^{1/2}a^{1/2}(1-\varepsilon^2)^{1/2}} \right]^2 - \left[\frac{e[1-\varepsilon \cos(\theta-\theta_0)]}{m^{1/2}a^{1/2}(1-\varepsilon^2)^{1/2}} \right]^2 \right\} \\ &= \frac{e}{a^{5/2}m^{1/2}(1-\varepsilon^2)^{5/2}} \frac{1}{\tau} \int_{\theta(t)}^{\theta(t+\tau)} d\theta (-1 + 3C\varepsilon - 3C^2\varepsilon^2 + 2S^2\varepsilon^2 + C^3\varepsilon^3 - 2CS^2\varepsilon^3) , \end{aligned} \quad (35)$$

where $\cos(\theta-\theta_0)$ and $\sin(\theta-\theta_0)$ were abbreviated by C and S in the last line.

Again treating that ε and θ_0 vary insignificantly during τ , at least as compared with $\theta(t)$, then there are only three terms in the integrand that do not fluctuate between negative and positive, namely, -1 , $-3C^2\varepsilon^2$, and $+2S^2\varepsilon^2$. The remaining terms after being integrated over and divided by τ , will be negligible. Thus, again for N of the order of 100 or more orbital periods,

$$\begin{aligned} & \frac{1}{\tau} \int_{\theta(t)}^{\theta(t+\tau)} d\theta (-1 + 3C\varepsilon - 3C^2\varepsilon^2 + 2S^2\varepsilon^2 + C^3\varepsilon^3 - 2CS^2\varepsilon^3) \\ & \rightarrow \frac{1}{NT} \int_{\theta(t)}^{\theta(t)+N2\pi} d\theta (-1 - 3C^2\varepsilon^2 + 2S^2\varepsilon^2) \\ & = \frac{1}{NT} (-N2\pi - 3N\pi\varepsilon^2 + 2N\pi\varepsilon^2) = \frac{1}{T} (-2\pi - \pi\varepsilon^2) . \end{aligned} \quad (36)$$

The result is

$$\left\langle \frac{2r^2 - (r\dot{\theta})^2}{r^3} \right\rangle \approx -\frac{e\pi(2+\varepsilon^2)}{a^{5/2}m^{1/2}(1-\varepsilon^2)^{5/2}T} . \quad (37)$$

Combining the numerator and denominator on the left side of (27), noting that T cancels out, and equating to our result on the right of $-\frac{1}{\omega_1}$,

$$\frac{\frac{2\pi}{a(1-\varepsilon^2)}}{-\left[\frac{e\pi(2+\varepsilon^2)}{a^{5/2}m^{1/2}(1-\varepsilon^2)^{5/2}}\right]} = -\frac{1}{\omega_1} . \quad (38)$$

Finally, the relation between the $n = 1$ period T_1 due to the CP wave ω_1 , and the period T_n of the n^{th} order subharmonic orbit, is $T_n = nT_1$, so the period for the $n = 2$ subharmonic resonance orbital is twice the period of the CP wave, etc. Moreover, for a classical electron in an elliptical orbit with semimajor axis a (Kepler-Coulomb result),

$$T = \frac{2\pi}{\left(\frac{e^2}{ma^3}\right)^{1/2}} , \quad (39)$$

so that

$$\omega_1 = \frac{2\pi}{T_1} = \frac{2\pi n}{T_n} = n \left(\frac{e^2}{ma_n^3}\right)^{1/2} , \quad (40)$$

where a_n is the semimajor axis of the orbit while in the n^{th} subharmonic resonance.

Combining, (38) reduces to

$$n = \frac{(2 + \varepsilon_{\text{crit},n}^2)}{2(1 - \varepsilon_{\text{crit},n}^2)^{3/2}} . \quad (41)$$

The label $\varepsilon_{\text{crit},n}$ was inserted here since this was deduced at the peak of the eccentricity curve, when $\left\langle \frac{d}{dt} \left[e(am)^{1/2} (1 - \varepsilon^2)^{1/2} \right] \right\rangle \approx 0$ in (25). Here, $n = 2, 3, 4, \dots$.

Numerical values can readily be solved for $\varepsilon_{\text{crit},n}$ in (41). Table 1 lists the first set of values of $\varepsilon_{\text{crit},n}$ for $n = 2, 3, \dots, 7$. Figure 7 plots these values of $\varepsilon_{\text{crit},n}$ up through $n = 20$, assuming that the orbit can be caught into a subharmonic resonance state. As can be seen for the $n = 2$ and 3 subharmonic resonance cases shown in Figs. 2 and 4, respectively, the first two values in Table 1 agree to three (Fig. 4) or four (Fig. 2) decimal places of the earlier simulation examples. Similar agreements with Table 1 are shown in [31] for $n = 4, 5, 6$.

n	$\varepsilon_{\text{crit},n}$
2	0.5542
3	0.6706
4	0.7316
5	0.7703
6	0.7975
7	0.8178

Table 1: $\varepsilon_{\text{crit},n}$ calculated for the first six (2, 3, ...,7) subharmonic resonances, assuming the orbit can be “caught”, starting with a circular orbit.

5 Concluding remarks

The hydrogen atom constitutes the simplest realistic physical system in atomic physics, which is probably why it has such a rich history of physical analysis [39]. The aim of the present work was to push this analysis yet farther, by examining previously unexplored and unexpected properties of hydrogen. The recognition of the properties uncovered here of extended states and quantized-like behavior of the simple classical hydrogen model, may well play a significant role in SED’s [8],[9],[10] ability to explain and describe atomic excited state phenomena. In addition, and perhaps surprisingly, but this new work should also enable new technological directions for storing information in atoms and for additional controlling mechanisms for physical processes like etching and ionization.

Here, we investigated the $n \geq 2$ subharmonic resonances in more detail, showing that a remains fairly constant during subharmonic resonance, while the semiminor axis b steadily decreases. When the orbit is initially circular, the eccentricity $\varepsilon = \left[1 - \left(\frac{b}{a}\right)^2\right]^{1/2}$ equals zero, but during subharmonic resonance, ε continues to increase until a critical value, $\varepsilon_{\text{crit},n}$, is reached. The analytic derivation for $\varepsilon_{\text{crit},n}$ in Sec. IV predicts new results, not deduced elsewhere. These values were also calculated via detailed simulation methods for $n = 2, 3, 4, 5, 6$ examples, producing agreement for the derived $\varepsilon_{\text{crit},n}$ values to several digits.

Thus, the analytic prediction in Sec. IV seem quite relevant for a deeper understanding of Rydberg dynamics. However, as mentioned, these predictions depend on: (1) the set of approximations that $E = \frac{1}{2}m\tilde{\mathbf{v}}^2 - \frac{e^3}{r} \approx -\frac{e^2}{2a}$, and $L_z = mr^2\dot{\theta} \approx e(am)^{1/2}(1 - \varepsilon^2)^{1/2}$, which seem sound for the situations examined here; (2) that time averages are taken over the fluctuations in E and L_z , due mainly to the CP plane wave action on the orbit, and (3) that $\langle \frac{d}{dt}L_z \rangle \approx 0$ when the subharmonic resonance condition changes to one of decay.

The material in [31] has additional information on this last point, showing that a_{initial} just needs to be slightly larger than a_n , otherwise $\langle \frac{d}{dt}L_z \rangle$ does

not have sufficient time to relax to zero. If the analysis in Sec. IV is to be criticized, it is likely on this last point, as it would be better to predict, via a more fundamental method, the point where resonance changes to decay. Nevertheless, the predictions shown here certainly seem of interest and are fairly close to detailed simulation results.

The phenomena predicted here is both quite different than past resonant Rydberg analysis, particularly for critical eccentricities, but also has much commonality. In particular, the $n = 1$ resonances discussed in [2]-[5], have similarities to the present subharmonic resonance examples. The $n = 1$ resonances can have fairly long resonance times, and are effected by A and α in interesting ways. However, as not discussed in earlier work, $n = 1$ resonances seem very “poor” at “catching” an electron, meaning, if an orbit decays into an $n = 1$ resonance position, rarely are the conditions such that the orbit turns into a long lasting resonance state. Indeed, the long lasting $n = 1$ states analyzed in [2], [4], and [5] were created with the orbit starting essentially already in the $n = 1$ state.

In contrast, the $n = 2$ and 3 cases are “generally quite good” at catching the electron, providing that A is above a critical value. However, for $n \geq 4$, the “poor catching” situation again arises; indeed, in [31], it was nontrivial in to come up with examples where such events can happen. Nevertheless, three examples were obtained for $n = 4, 5, 6$, but only by making the initial orbit to be slightly elliptical. Evidently, for these higher values of n , difficulty arises in finding values of a_{initial} and $\varepsilon_{\text{initial}}$ to enable the “catch” and subsequent resonance to occur.

Moreover, it should be noted that when the classical electron has been in an n subharmonic resonance, and eventually falls back into orbital decay, the orbit will decay through the $n - 1$ subharmonic resonance, the $n - 2$ subharmonic resonance, etc. Only if the conditions are just right will a second “catch” occur. The effects of these resonances can clearly be seen as “blips” in the decaying orbital behavior (examples are shown in [31]), but second “catches” are either most rare, or possibly nonexistent.

Regarding what precisely enables “capture,” the key parameters are certainly: (1) A , as this ultimately dictates how much energy can be pumped into the orbit to offset the constant, but small rate of energy loss due to radiation reaction; (2) the phase difference α between the initial velocity vector and the CP electric field; (3) the initial ε of the orbit as it nears or enters the resonance, and the initial value of a before decaying into the resonance point. However, more important than this simple listing of parameters is the “power” $\tilde{\mathbf{F}} \cdot \tilde{\mathbf{v}}$, versus t , where $\tilde{\mathbf{F}}$ is the sum of the Lorentz force due to electromagnetic radiation, and the largely resistive, but weak, radiation reaction force. A typical plot of $\tilde{\mathbf{F}} \cdot \tilde{\mathbf{v}}$ versus t , is shown in [31]. During a $n \geq 2$ subharmonic resonance, there are approximately n sign changes of $\tilde{\mathbf{F}} \cdot \tilde{\mathbf{v}}$ in each orbit, in addition to magnitude changes. Hence, over several several hundred orbits, this plot appears fairly stochastic in nature, and is very different in behavior than the $n = 1$ resonances discussed in earlier references [2],[4],[5], where the time between sign changes of $\tilde{\mathbf{F}} \cdot \tilde{\mathbf{v}}$ may last tens to hundreds of orbits, as opposed to $\frac{1}{n}$ times a single orbital

period for a subharmonic resonance. Plots like Fig. 5 in [2] and Fig. 3 in [4] show this effect for $n = 1$; they are in sharp contrast to the situation for $n \geq 2$.

Thus, the $n \geq 2$ situations are typically many times more complicated than the $n = 1$ case. At first blush, there should be some surprise that there is any resonance at all for $n \geq 2$, but there is, and in certain cases, such as $n = 2$ and 3, the resonance is quite significant, of long duration, and able to “catch” decaying orbits under a variety of conditions. Ultimately, it comes down to a statistical analysis averaging over the “energy in” and “energy out” periods, with the former being larger during resonances, before final decay begins. Such predictive calculations are not easy to deduce, and hence the large reliance on simulation here.

Possibly why the $n = 2$ and 3 subharmonic resonances more easily catch a decaying orbit, than for $n = 1$, is that the $n = 2$ and 3 situations provide rapid plus and minus power contributions in every orbit. If the phase is not quite right at first, then over a series of such fluctuations, one or more may eventually provide the right input power to put the orbit onto a resonance path. In contrast, for the case of $n = 1$, the scenario is quite different, as positive and negative power inputs to the orbit last over tens to hundreds of orbits. This conjecture could readily be tested in future work. Two key factors here are that (1) the orbit is of course altered by the CP wave, and the (2) CP force and electron velocity must be in sync, at least on average, for a net power input to be created to compensate the radiation reaction effects.

Some other points should be mentioned. Clearly the emphasis here has been on a single CP wave, as opposed to a linear polarization, or, more generally, an incident electromagnetic radiation with arbitrary elliptical polarization. The reason for focusing on CP waves is of several fold. First, as studied in [2] with a CP wave, “ideally” one can obtain a perfect balance with the radiation reaction, and can then proceed from there to study deviations from this condition. For this reason, some of the initial physical behavior for balance and resonance seems easier to examine with CP waves. Second, any radiation field can be decomposed into CP waves, just as readily as with plane waves. Third, if one does examine, via simulation, just linear or more general elliptically polarized radiation, it turns out that the “signatures” of resonance show up here as well, as in [3]. But, admittedly, the full scope of these other conditions has not been fully examined here.

How might these results be utilized? Summarizing earlier points, for a true Rydberg atomic system, where the outer electron is nearly ionized, the quantum energy states of the outer electron are essentially a continuum. The classical physics analysis studied here, should hold fairly well for much of this phenomena. Evidently, an electron can be held in a classical subharmonic resonance with an incident CP laser beam, for fairly long times. By taking advantage of subharmonic resonances, and developing novel schemes for their control, it is possible that new means for reading and writing information to atoms can be realized. Similarly, controlling plasma-like states for etching, display, etc., via strategies not taken before, may be possible. Undoubtedly such controls will likely be of the statistical process control type, since atoms of

different initial conditions, even slightly different, will certainly not all respond the same way. Ensemble variations would need to be taken into account. Thus, the subharmonic resonances for hydrogen and Rydberg atoms could provide interesting possibilities for technology applications.

More fundamentally, however, the work analyzed here may provide a partial basis for the origin of excited atomic state phenomena via the classical theory of SED. Large duration quasi-stable states for classical resonances of Rydberg and hydrogen atoms were shown to naturally occur, with quantized-like eccentricities of orbits created prior to orbital decay. Of course, this study was done with only a single CP wave, such as might occur with a strong laser light shining on an atom. To fold these ideas into SED would require the important inclusion of ZP radiation at $T = 0$, which would introduce considerable stochastic behavioral changes. Nevertheless, it seems quite possible that classical resonances related to those examined here, but that include the effects of an applied light source plus the background radiation spectrum, will be essential to consider.

Thus, previously neglected subharmonic resonance phenomena, can clearly play a prominent role in classical hydrogen dynamics. They may also contribute in significant ways to “excited state phenomena” within the framework of SED. Using a rough QM description, excited states in atomic physics are quasi-stable states that are closely effected by spontaneous emission due to the vacuum and stimulated emission due to applied radiation of the right frequency. SED, although a classical physical theory, certainly has these features of zero-point and applied radiation, but to date, except for the expected stable ground state, quasi-stable atomic states has not been closely examined.

Acknowledgements

I thank Dr. Lu Gao for using the code described here to carry out an independent study with me, some time ago, to explore some of the early beginnings of the work reported here. I also thank Professor Timothy Boyer for a recent, enjoyable morning of discussing the results in a first draft of this article and for his ideas on why the $n = 1$ versus $n = 2$ and 3 resonances behave differently in terms of being able to “catch” the classical electron.

Figures

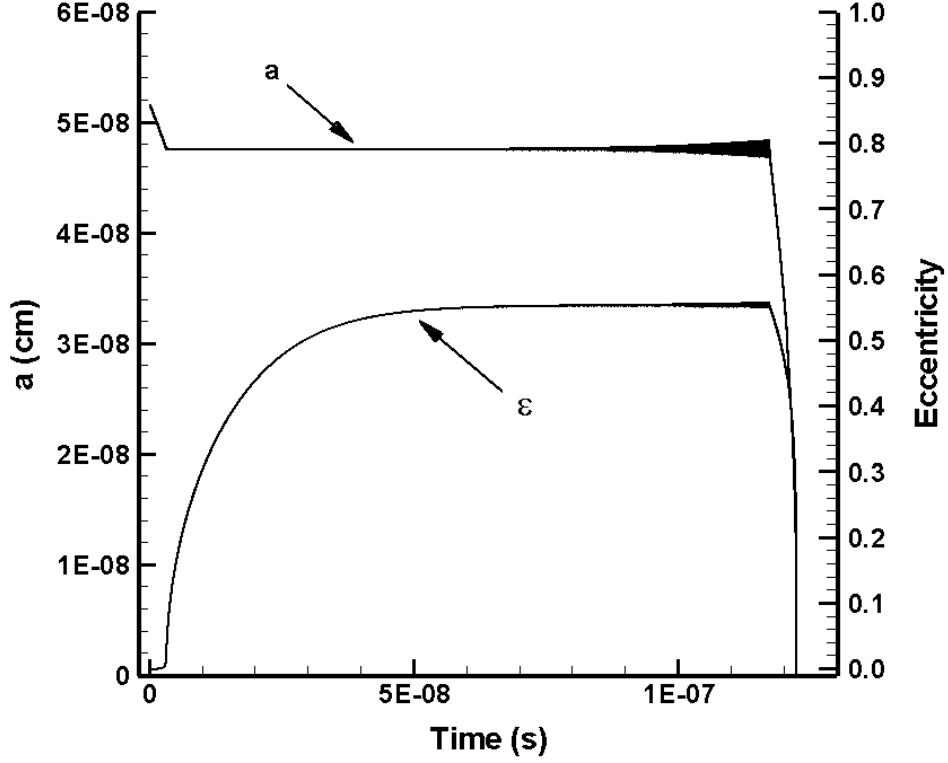


Fig. 1 This $n = 2$ subharmonic resonance condition has $a_1 = 3.0 \text{ \AA}$ and $a_2 = a_1 2^{2/3} = 4.7622 \text{ \AA}$, while $A = 50 \text{ statvolt/cm}$, $\varepsilon_{\text{initial}} = 0$, and $\alpha = 0$, where α is the initial phase α between the CP wave and the orbit. The ε vs. t curve is also shown. The orbit starts as circular, with $a(t)$ decreasing until the $n = 2$ resonance is reached at $a = 4.7622 \text{ \AA}$. A long resonance sets in, during which time the orbit becomes more and more elliptical, changing from $\varepsilon = 0$ to $\varepsilon \approx 0.554$, at which point orbital decay sets in.

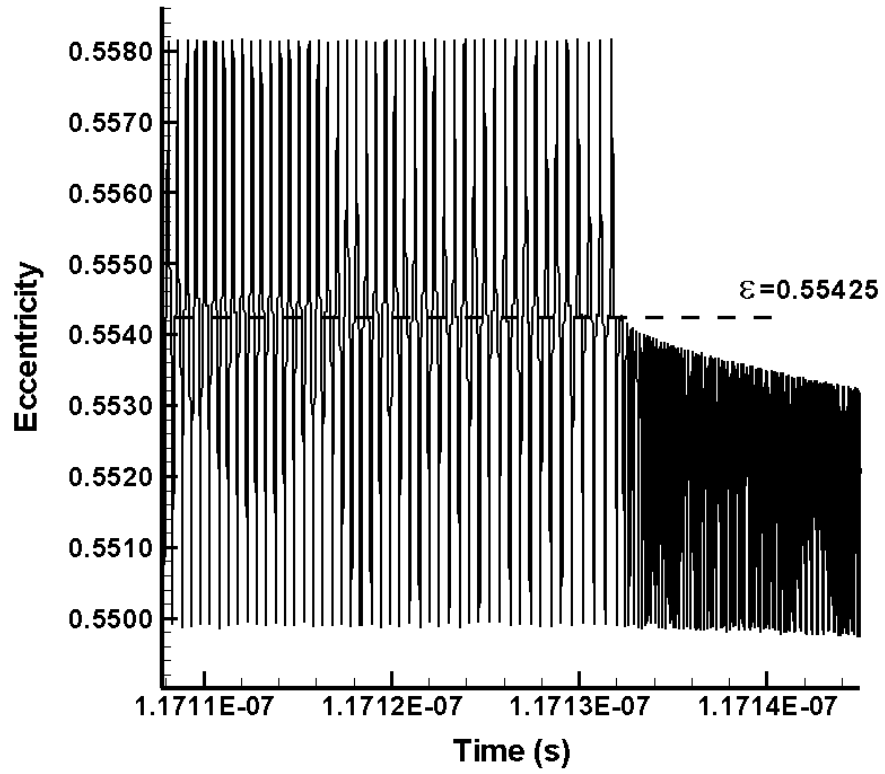


Fig. 2 This plot of $\varepsilon(t)$ vs. t , focuses in at the point in Fig. 1 where the orbit changes from one of resonance to orbital decay.

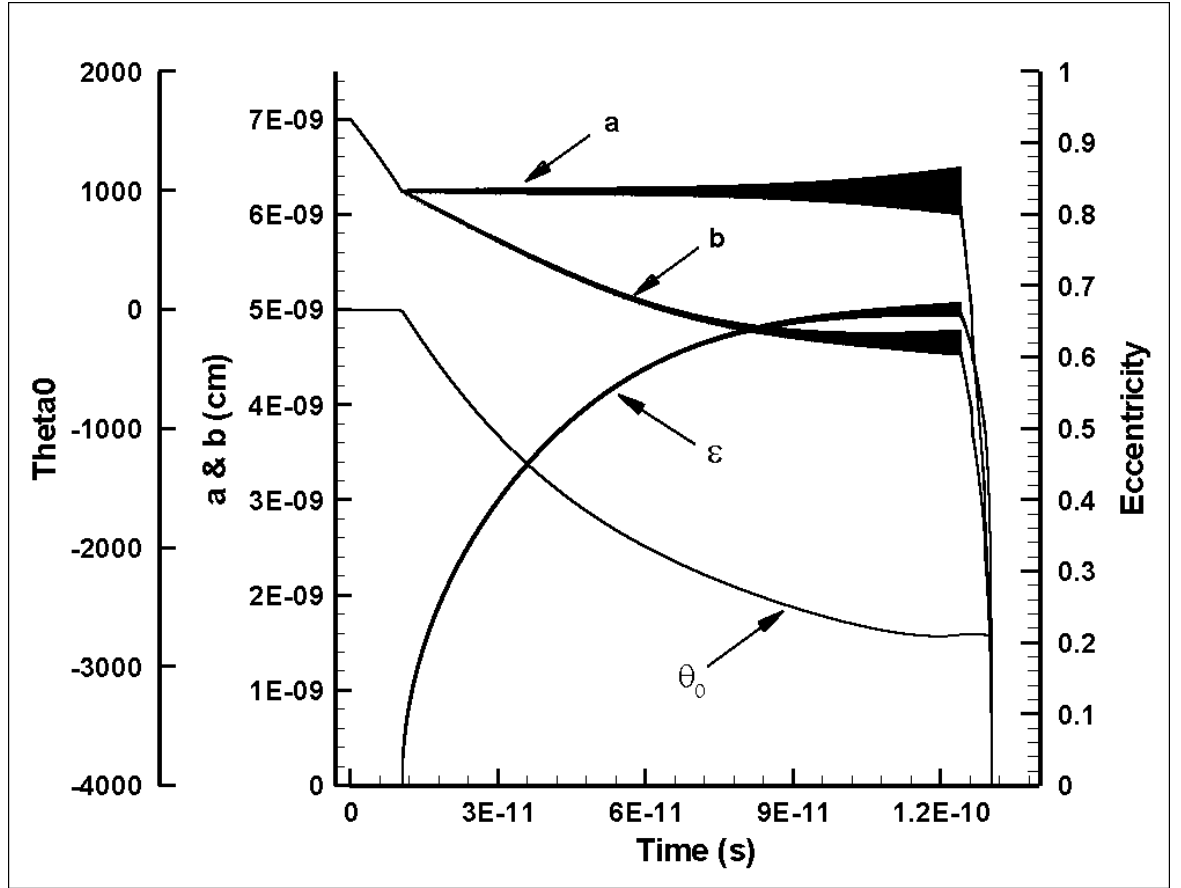


Fig. 3 Here, $A = 35,000$ statvolt/cm, $a_1 = 0.3 \text{ \AA}$, $a_3 = 0.3 \times 3^{2/3} \text{ \AA} = 0.6240 \text{ \AA}$, $a_{\text{initial}} = 0.7 \text{ \AA}$, $\varepsilon_{\text{initial}} = 0$, and $\alpha = 0$ in (12) and (13). The classical electron orbit begins in a spherical orbit at $a = 0.7 \text{ \AA}$, but upon hitting resonance at $a_3 = 0.6240 \text{ \AA}$, the orbit sharply transitions into one of resonance, where a remains “constant with growing fluctuations,” for about 1.2×10^{10} s, until orbital decay starts. $a(t)$, $b(t)$, $\varepsilon(t)$, and $\theta_0(t)$ are shown in this plot.

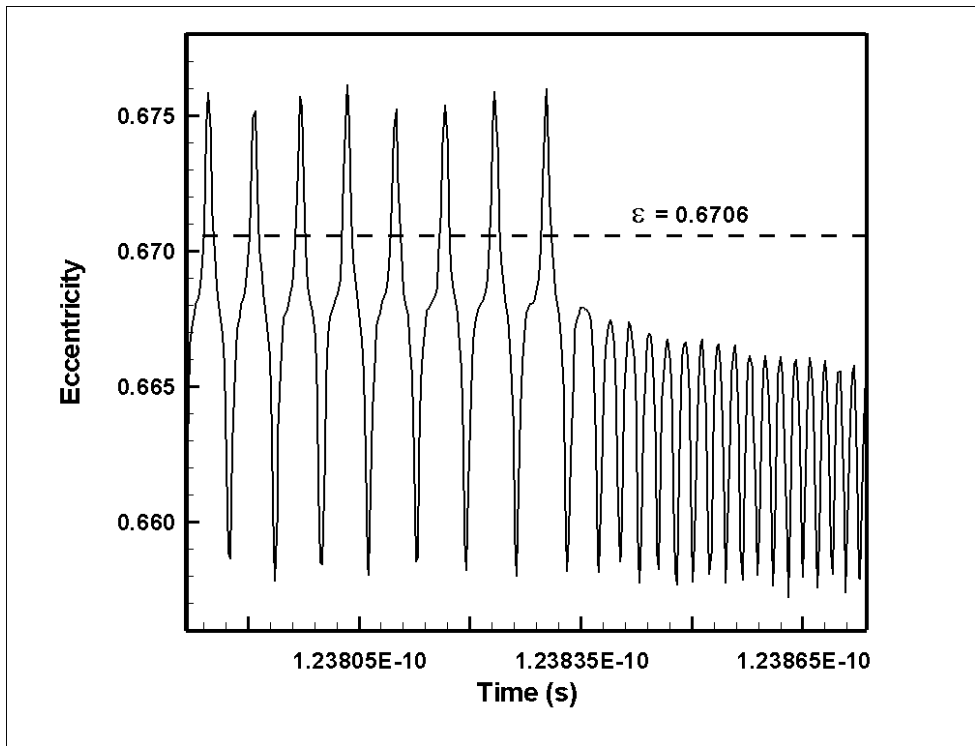


Fig. 4 This plot shows the behavior of ε vs. t at the point where the $n = 3$ resonance condition in Fig. 3 changes to orbital decay.

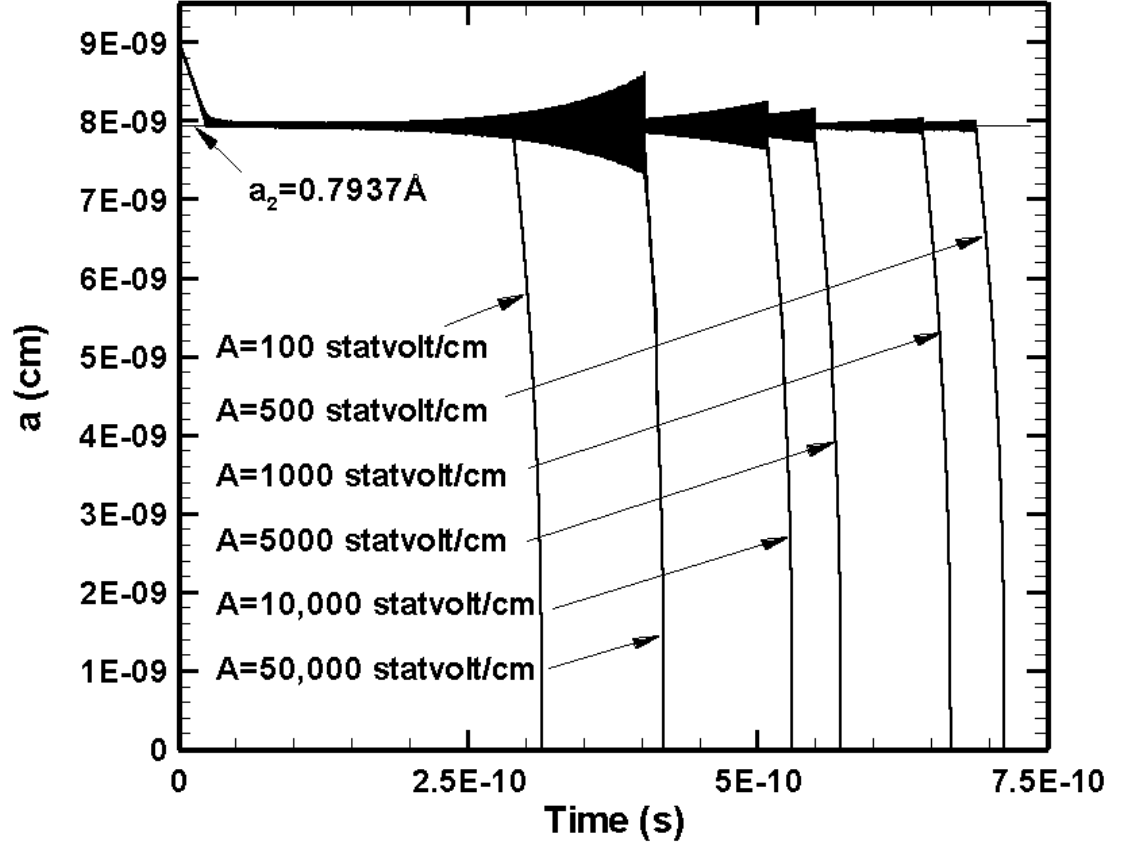


Fig. 5 Here a range of CP amplitude A values (100, 500, 1000, 5000, 10,000, and 50,000 statvolt/cm) are simulated for the conditions of the CP wave's angular velocity being $\omega_1 = \left(\frac{e^2}{ma_1^3}\right)^{1/2}$, with $a_1 = 0.5 \text{ \AA}$. In each case the starting radius is 0.90 \AA , with $\varepsilon_{\text{initial}} = 0$, $\alpha = 0$. The resonance encountered here is $n = 2$, $a_2 = a_1 2^{2/3} = 0.7937 \text{ \AA}$. As can be seen, all situations have a strong resonance at this a_2 value, with the main difference being twofold: (1) the larger A is, the larger the envelope of oscillations of a about a_2 ; (2) A can clearly effect the duration time in this $n = 2$ subharmonic resonance.

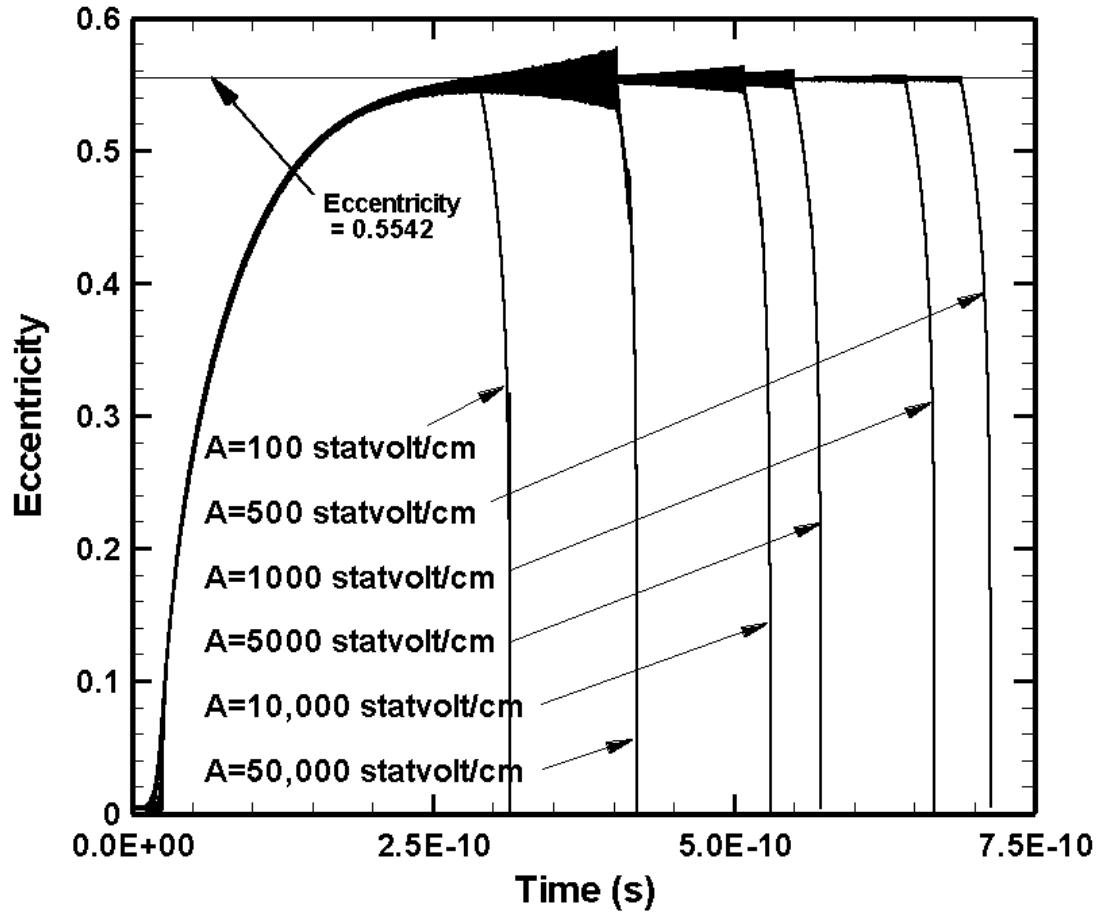


Fig. 6 The same simulation conditions as in Fig. 5 also here, but now ε vs. t is plotted for each of the six A values examined of 100, 500, 1000, 5000, 10,000, and 50,000 statvolt/cm. All curves show that $\varepsilon_{\text{crit},2} \approx 0.5542$. This result occurred despite the difference of 500 factor difference in A values, from 100 to 50,000 statvolt/cm. Other behaviors differed, such as the envelope size of the fluctuations in ε , and the length of time in resonance, but $\varepsilon_{\text{crit},2}$ was largely independent of A , much like a_2 was common for all the curves in Fig. 5.

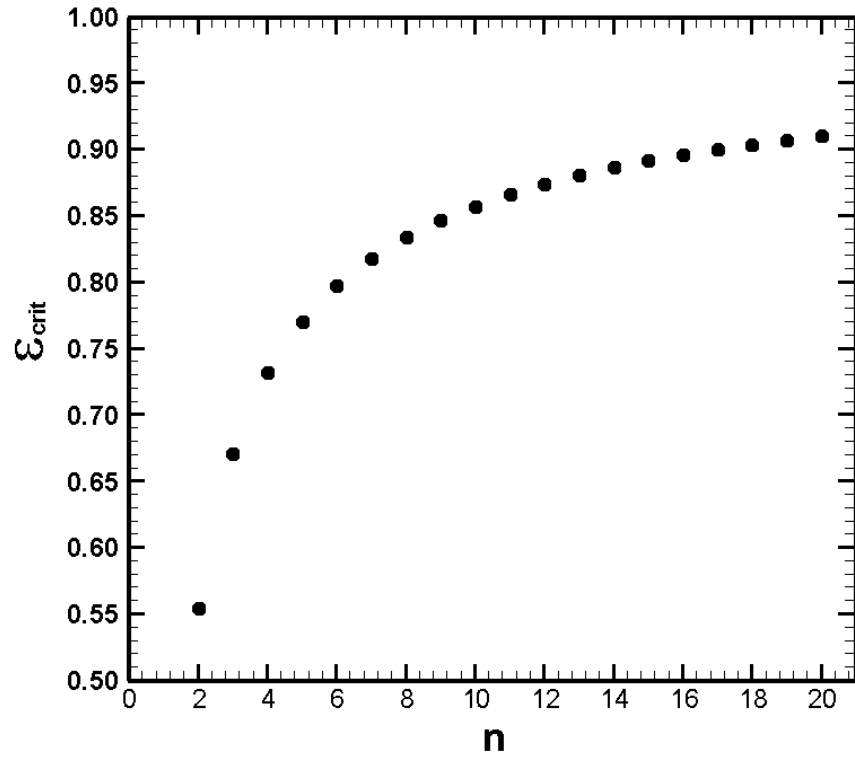


Fig. 7 Plot of $\epsilon_{crit,n}$ vs. n , where n represents the subharmonic resonance level. The first six values are in Table 1.

References

- [1] D. Cole and Yi Zou. Subharmonic resonance behavior for the classical hydrogen atomic system. *J. Sci. Comput. (USA)*, 39(1):1 – 27, 2009/04/.
- [2] D.C. Cole and Y. Zou. Simulation study of aspects of the classical hydrogen atom interacting with electromagnetic radiation: Circular orbits. *Journal of Scientific Computing*, 20(1):43 – 68, 2004.
- [3] D. C. Cole and Y. Zou. Simulation study of aspects of the classical hydrogen atom interacting with electromagnetic radiation: Elliptical orbits. *Journal of Scientific Computing*, 20(3):379–404, 2004.
- [4] D. C. Cole and Y. Zou. Perturbation analysis and simulation study of the effects of phase on the classical hydrogen atom interacting with circularly polarized electromagnetic radiation. *Journal of Scientific Computing*, 21(2):145–172, 2004.
- [5] D. C. Cole and Y. Zou. Analysis of orbital decay time for the classical hydrogen atom interacting with circularly polarized electromagnetic radiation. *Phys. Rev. E*, 69(1):016601–1–12, 2004/01/.
- [6] D. C. Cole and Y. Zou. Quantum mechanical ground state of hydrogen obtained from classical electrodynamics. *Physics Letters A*, 317(1–2):14–20, Oct. 13, 2003.
- [7] M. W. Noel, W. M. Griffith, and T. F. Gallagher. Classical subharmonic resonances in microwave ionization of lithium rydberg atoms. *Phys. Rev. A*, 62:063401, 2000.
- [8] T. H. Boyer. General connection between random electrodynamics and quantum electrodynamics for free electromagnetic fields and for dipole oscillator systems. *Phys. Rev. D*, 11(4):809–830, 1975.
- [9] D. C. Cole. Reviewing and extending some recent work on stochastic electrodynamics. In A. Lakhtakia, editor, *Essays on the Formal Aspects of Electromagnetic Theory*, pages 501–532. World Scientific, Singapore, 1993.
- [10] L. de la Peña and A. M. Cetto. *The Quantum Dice - An Introduction to Stochastic Electrodynamics*. Kluwer Acad. Publishers, Kluwer Dordrecht, 1996.
- [11] T. W. Marshall. Statistical electrodynamics. *Proc. Camb. Phil. Soc.*, 61:537–546, 1965.
- [12] T. H. Boyer. Derivation of the blackbody radiation spectrum without quantum assumptions. *Phys. Rev.*, 182:1374–1383, 1969.
- [13] D. C. Cole. Derivation of the classical electromagnetic zero–point radiation spectrum via a classical thermodynamic operation involving van der waals forces. *Phys. Rev. A*, 42:1847–1862, 1990.

- [14] T. H. Boyer. Thermal effects of acceleration through random classical radiation. *Phys. Rev. D*, 21(8):2137–2148, 1980.
- [15] T. H. Boyer. Thermal effects of acceleration for a classical dipole oscillator in classical electromagnetic zero-point radiation. *Phys. Rev. D*, 29(6):1089–1095, 1984.
- [16] D. C. Cole. Properties of a classical charged harmonic oscillator accelerated through classical electromagnetic zero-point radiation. *Phys. Rev. D*, 31(8):1972–1981, 1985.
- [17] D. C. Cole. Thermal effects of acceleration for a spatially extended electromagnetic system in classical electromagnetic zero-point radiation: Transversely positioned classical oscillators. *Phys. Rev. D*, 35:562–583, 1987.
- [18] T. H. Boyer. Temperature dependence of van der waals forces in classical electrodynamics with classical electromagnetic zero-point radiation. *Phys. Rev. A*, 11:1650–1663, 1975.
- [19] D. C. Cole. Correlation functions for homogeneous, isotropic random classical electromagnetic radiation and the electromagnetic fields of a fluctuating classical electric dipole. *Phys. Rev. D*, 33:2903–2915, 1986.
- [20] D. C. Cole. Entropy and other thermodynamic properties of classical electromagnetic thermal radiation. *Phys. Rev. A*, 42:7006–7024, 1990.
- [21] D. C. Cole. Reinvestigation of the thermodynamics of blackbody radiation via classical physics. *Phys. Rev. A*, 45:8471–8489, 1992.
- [22] T. W. Marshall. Random electrodynamics. *Proc. R. Soc. London, Ser. A*, 276:475–491, 1963.
- [23] T. H. Boyer. Diamagnetism of a free particle in classical electron theory with classical electromagnetic zero-point radiation. *Phys. Rev. A*, 21(1):66–72, 1980.
- [24] T. H. Boyer. Random electrodynamics: The theory of classical electrodynamics with classical electromagnetic zero-point radiation. *Phys. Rev. D*, 11(4):790–808, 1975.
- [25] Theo M Nieuwenhuizen and Matthew T P Liska. Simulation of the hydrogen ground state in stochastic electrodynamics. *Physica Scripta*, 2015(T165):014006, 2015.
- [26] Theodorus M. Nieuwenhuizen and Matthew T. P. Liska. Simulation of the hydrogen ground state in stochastic electrodynamics-2: Inclusion of relativistic corrections. *Foundations of Physics*, 45(10):1190–1202, 2015.
- [27] Theodorus M. Nieuwenhuizen. On the stability of classical orbits of the hydrogen ground state in stochastic electrodynamics. *Entropy*, 18(4):135, 2016.

- [28] T.H. Boyer. Classical zero-point radiation and relativity: The problem of atomic collapse revisited. *arXiv: 1511.02083v1*, pages 1–15, 2015.
- [29] P. M. Koch and K. A. H. van Leeuwen. The importance of resonances in microwave “ionization” of excited hydrogen atoms. *Physics Reports*, 255:289–403, 1995.
- [30] H. Maeda, D. V. L. Norum, and T. F. Gallagher. Microwave manipulation of an atomic electron in a classical orbit. *Science*, 307:1757–1760, March 18, 2005.
- [31] D.C. Cole. 2017. See the, "Electronic supplementary material," at [URL will be inserted by publisher]. This material contains a number of additional simulations that complement and provide additional insight to the main article. In particular, simulations for subharmonic resonances of $n=4,5,6$ are shown, along with the critical eccentricities that arise.
- [32] C. Teitelboim, D. Villarroel, and Ch. G. van Weert. Classical electrodynamics of retarded fields and point particles. *Riv. del Nuovo Cimento*, 3(9):1–64, 1980.
- [33] John David Jackson. *Classical Electrodynamics*. John Wiley & Sons, 2nd edition, 1975.
- [34] G. N. Plass. Classical electrodynamic equations of motion with radiative reaction. *Rev. Mod. Phys.*, 33(1):37–62, 1961.
- [35] W. H. Press, S. A. Teukolsky, W. T. Vetterling, and B. P. Flannery. *Numerical Recipes in C: The Art of Scientific Computing*. Cambridge University Press, New York, second edition, 1992.
- [36] H. Goldstein. *Classical Mechanics*. Addison–Wesley, Reading, MA, second edition, 1981.
- [37] T. L. Chow. *Classical Mechanics*. John Wiley & Sons, Inc., New York, 1995.
- [38] R. A. Becker. *Introduction to Theoretical Mechanics*. McGraw-Hill, New York, 1954.
- [39] J. S. Rigden. *Hydrogen: The Essential Element*. Harvard University Press, Cambridge, Massachusetts, 2002.

**Supplemental document to the article in European Physical
Journal D, “Subharmonic resonance and critical eccentricity for
the classical hydrogen atomic system,” by Daniel C. Cole**

Email: dccole@bu.edu

Affiliation: Boston University, Department of Mechanical Engineering

I. INTRODUCTION

The information in the present document supplements the main material contained in the article entitled, “Subharmonic resonance and critical eccentricity for the classical hydrogen atomic system,” published in Foundations of Physics, and written by Daniel C. Cole. Please note that the numbering of the figures in this document will start with Fig. 8, and continue with Figs. 9, 10, etc., as if the figure numbering was continuing in sequence from the main paper that is referenced here, which ended with Fig. 7.

Section II of the present supplementary material provides some additional information on subharmonic resonances, particularly for $n = 2$ situations. Several subtleties exist for these subharmonic resonance behaviors. One of the most important points is an examination of the rapid variation in time of the power fed into, and taken out of, the orbiting classical electron via the CP wave and the radiation reaction. Figure 8f shows this information, which really governs when a sustained subharmonic resonance can occur, and why orbital decay eventually takes place.

Section III then turns to comparisons of $E = \frac{1}{2}m\tilde{\mathbf{v}}^2 - \frac{e^3}{r}$ versus $-\frac{e^2}{2a}$, as well as $L_z = mr^2\dot{\theta}$ versus $e(am)^{1/2}(1 - \varepsilon^2)^{1/2}$. The approximations of $E = \frac{1}{2}m\tilde{\mathbf{v}}^2 - \frac{e^3}{r} \approx -\frac{e^2}{2a}$ and $L_z = mr^2\dot{\theta} \approx e(am)^{1/2}(1 - \varepsilon^2)^{1/2}$ were made in Sec. IV of the main article, so an examination of these approximations is of course important to tackle, as done here (Figs. 12a,b,c). The approximations are typically shown to be quite good for the situations examined in the main article. Section III then examines what happens to L_z when a_{initial} is very close to a subharmonic resonance and how this can impact the degree of accuracy of the numbers in Table 1 of the main article for $\varepsilon_{\text{crit},n}$. As will be shown in Figs. 13,a,b,c, if a_{initial} is very close to a_n , the transition from resonance to decay will occur before $\langle \frac{d}{dt}L_z \rangle$ reaches zero, which effects an assumption made in the derivation in Sec. IV of the main article. As shown here, this was a key factor in why some values in Table 1 agreed with detailed simulations to four digits, while others agreed to only two and three digits.

Section IV next provides examples of subharmonic resonances for $n = 4, 5, 6$. These examples were certainly more difficult to come up with than the earlier examples of $n = 2$ and 3, which in comparison, were quite easy to construct. We conjecture here why the $n = 4, 5, 6$ cases, and presumably for $n = 7, 8, \dots$, as well, are more difficult in terms of “catching” a classical electron during its orbital decay. Section V ends with a brief summary

of the material here.

II. MORE DETAILED INFORMATION FOR SUBHARMONIC RESONANCES, PARTICULARLY $n = 2$

Figures 8a-f illustrate in some detail most of the essential points of the main article. Figures 8a-f pertain to one arbitrary $n = 2$ subharmonic resonance simulation. In each of these figures, the classical electron was started in a circular orbit, with radius 1.08 \AA . Now, to be really classical, where quantum effects would be minimized, then it is true that this orbit should be chosen much larger, as was done in Figs. 1 and 2 in the main article. However, the same effect illustrated here will still occur if the Lorentz-Dirac equation [1],[2] is taken to be the governing equation of motion, as has been verified by numerous simulation tests of ours; the only restriction is that one should expect this subharmonic resonance to hold, physically, at the larger radius connections, where the correspondence principle provides the connection between large quantum numbers and continuous classical trajectories. The reason for showing smaller radii is that simulations certainly run much faster at small radii, plus if SED is to be explored further to understand better about its applicability and deficiencies, then the smaller radii are of most interest.

In Fig. 8a, the y-axis shows the semimajor, a , and semiminor, b , axes of the classical electron's orbit. Since the orbit starts in a circle, then $a \approx b$, up until $t \approx 0.42 \times 10^{-10} \text{ s}$. There are about classical 10^5 orbits up until the resonance point at $t \approx 0.42 \times 10^{-10} \text{ s}$. During each orbit, energy in the form of classical electromagnetic radiation is constantly given off, resulting in the orbit constantly decreasing from $a = 1.08 \text{ \AA}$ to about 0.9524 \AA , where the $n = 2$ subharmonic resonance abruptly occurs. Note that during this entire simulation, a circularly polarized plane wave is constantly acting, however, it has a very weak effect on the trajectory until a decreases to the resonance point, at which time a very sharp resonance can be seen. In this simulation, the amplitude of the electric field of the CP wave was chosen to be $A = 1000 \text{ statvolt/cm}$, in cgs units. The angular frequency of the CP wave, in this simulation, is given by $\omega_1 = \left(\frac{e^2}{ma_1^3}\right)^{1/2}$, where, again in cgs units, the charge of the classical electron is $e = 4.80298 \times 10^{-10} \text{ esu}$, the mass of the electron is $m = 9.1091 \times 10^{-28} \text{ g}$, and here a_1 , for this simulation, was chosen to be $0.6 \text{ \AA} = 0.6 \times 10^{-8} \text{ cm}$. Thus, $\omega_1 = 3.4241 \times 10^{16} \text{ s}^{-1}$. The $n = 2$ net angular frequency resonance, when a CP wave is applied with an angular

frequency ω_1 , is given by $\omega_2 = \frac{\omega_1}{2}$, which occurs if $\omega_2 = \left(\frac{e^2}{ma_2^3}\right)^{1/2} = \frac{1}{2}\omega_1 = \frac{1}{2}\left(\frac{e^2}{ma_1^3}\right)^{1/2}$, or $a_2 = a_1 \times 2^{2/3}$. For this simulation, that means $a_2 = 0.6 \text{ \AA} \times 2^{2/3} \approx 0.9524 \text{ \AA}$. As can be seen from Fig.8a, this is precisely where this resonance takes place, and indeed holds to many decimal places if we were to zoom in on the plot much closer.

At this point, the applied CP wave has a clear effect on the orbit. The semimajor axis a no longer decays, but stays fairly constant, while the semiminor axis, b , begins a steady decline. The orbit abruptly changes from a circular one ($\varepsilon = 0$) during the initial decay period between $0 \leq t \lesssim 0.42 \times 10^{-10} \text{ s}$, to becoming more and more elliptical between $0.42 \times 10^{-10} \text{ s} \lesssim t \lesssim 1.07 \times 10^{-9} \text{ s}$. Figure 8b shows this behavior. During this resonance period, about 2.8×10^6 orbits occur, each with a period of approximately $3.67 \times 10^{-16} \text{ s}$.

Each of the curves, a vs. t , b vs. t , and ε vs. t , contain a fluctuation to them that increasingly grows larger with time. This can be seen by the increasing “blocky” width of each of these lines gradually increasing from the point of resonance $t \approx 0.42 \times 10^{-10} \text{ s}$, to when decay eventually sets in at about $t \approx 1.07 \times 10^{-10} \text{ s}$. This growing width of each of these three curves contains a very fine oscillating line, growing in amplitude as time increases. To illustrate, Fig. 8c focuses closely in on a vs. t at $t \approx 8 \times 10^{-10} \text{ s}$, where a periodic oscillation of a vs. t is seen, constituting the source of the blocky curve in Fig. 8b that grows in width until the decay point is finally reached. The oscillatory nature of a vs. t for this $n = 2$ subharmonic resonance has many similar features to the $n = 1$ resonance analyzed in detail in Refs. [3],[4],[5], in that as A grows, the period of the oscillation in Fig. 8c decreases and the amplitude of the oscillations increases.

Other than the magnitude of A effecting the fluctuation amplitude of $a(t)$, most other features of this resonance remain independent of A (provided it is above a critical value), namely: the resonance at $a_2 = 0.9524 \text{ \AA}$ still occurs at this precise value of $a_1 n^{2/3}$, where $n = 2$; the center of the a vs. t slightly fluctuating curve remains quite flat; and resonance stands out as a clear feature, although decay always eventually sets in. The time in resonance before decay sets in certainly depends on A as well as the initial phase α between the CP wave and the orbit, all very similar to the studies carried out on primary ($n = 1$) resonance in previous studies [4],[5], where the orbital and CP wave period are essentially the same. In addition, the length of time in resonance also depends on the starting point of a (*i.e.*, a_{initial}) above the resonance point, and if the initial orbit is circular or has some degree of

ellipticity.

Figure 8d examines the basic behavior of the eccentricity. When resonance sets in, ε increases in value as the orbit becomes more elliptical. Also, the ε vs. t curve widens in width as the decay point is approached, due to the increasing oscillation amplitude of ε . After the decay transition point and the orbit changes from one of resonance to that of decay, ε decreases rapidly toward zero, meaning a circular orbit, as discussed in [6].

Figure 8e clarifies some of the points on fluctuations of $\varepsilon(t)$, as it examines the point in Fig. 8d where orbital decay begins. The oscillations of ε are largest right before the decay point. A critical change occurs when the larger oscillations to the left “close over at the top,” becoming smaller humped oscillations on the right, that now decrease in both amplitude and average value. From this point on, the CP plane wave loses its ability to remain in phase with the orbit. The amount of CP positive energy pumped into the orbit decreases, on average, while the amount of CP negative work increases, as seen in the degree that the CP electric field pushes and opposes the electron along its trajectory. Thus, for $1.07385 \times 10^{-10} \text{ s} \lesssim t$, the CP electric field provides a net positive energy contribution, on average, to compensate the small, but constant radiation reaction zapping of energy. After $t = 1.07385 \times 10^{-10} \text{ s}$, the radiation reaction on the electron results in the orbit returning to one of steady decay, as the CP wave becomes sufficiently out of phase with the orbit to provide adequate compensation. If we were to show the oscillations in the decaying curve farther out to the right in Fig. 8e, they become smaller and smaller, the farther away from the resonance point.

However, perhaps the most interesting point of Fig. 8e is the value $\varepsilon_{\text{crit},n} \approx 0.5542$, for this $n = 2$ simulation. It turns out that whether we repeat this simulation for $a_2 = 2 \text{ \AA}$, 10 \AA , 20 \AA , etc., $\varepsilon_{\text{crit},2}$ is independent of the subharmonic resonance point, for the case of an initial circular orbit that decays into the resonance point, as deduced analytically in Sec. IV of the main article. This remarkable property appears to hold for all other $n = 2$ situations, aside from a few points to be discussed later in this supplemental document.

Figure 8f shows two plots, the top one being the potential plus kinetic energy of, $E(t) = -\frac{e^2}{r(t)} + \frac{1}{2}m|\tilde{\mathbf{v}}(t)|^2$, as a function of time, t , where r is the radial distance to the nucleus and $\tilde{\mathbf{v}}$ is the classical electron’s velocity. The bottom curve is $\tilde{\mathbf{F}} \cdot \tilde{\mathbf{v}}$ vs. t , where $\tilde{\mathbf{F}}$ is the sum of the CP wave and radiation reaction forces. The narrow time region shown in Fig. 8f of $2.65 \times 10^{-13} \text{ s}$ (same interval as in Fig. 1e) encompasses the moment when the orbit in Fig.

8b changes from one of resonance to that of decay.

The top curve in Fig. 8f of $-\frac{e^2}{r(t)} + \frac{1}{2}m|\tilde{\mathbf{v}}(t)|^2$, closely matches the approximate energy $-\frac{e^2}{2a(t)}$, where $a(t)$ is of course the relatively slowly changing semimajor axis of the approximate elliptical orbit, as the elliptical orbit slowly grows and shrinks. Indeed, at the scale in Fig. 1f, $E(t) = -\frac{e^2}{r(t)} + \frac{1}{2}m|\tilde{\mathbf{v}}(t)|^2$ and $-\frac{e^2}{2a(t)}$, are virtually indistinguishable from each other. This fact will be illustrated more clearly later in Figs. 12a and 12b, and was used to advantage in Sec. IV of the main article, when analytically deducing values for $\varepsilon_{\text{crit},n}$.

For the situation of Fig. 8f, in resonance, $a \approx a_2 = 0.6 \times 2^{2/3} \text{ \AA} = 0.9524 \text{ \AA}$, with a small oscillation of about $\pm 1.4\%$ (this was measured by zooming in on Fig. 8b) about this value at the onset of orbital decay, so the center of E vs. t is very close to $-\frac{e^2}{2a_2} = -1.211 \times 10^{-11}$ erg, as can be seen in the top curve in Fig. 8f.

The bottom curve in Fig. 8f is the work per unit time put into the trajectory. When in resonance, the sign of this curve changes roughly n times per orbit when in an n^{th} subharmonic resonance, since the orbital period is close to n times the period of the CP wave. With about 720 orbital periods in the 2.65×10^{-13} s time interval in Fig. 8f, and roughly twice as many sign changes in $\tilde{\mathbf{F}} \cdot \tilde{\mathbf{v}}$ for this $n = 2$ subharmonic resonance, the plot of $\tilde{\mathbf{F}} \cdot \tilde{\mathbf{v}}$ vs. t in the bottom of Fig. 8f is quite complicated, considerably more so than $n = 1$ resonance situations discussed in earlier references [3],[4],[5], where the times between sign changes of $\tilde{\mathbf{F}} \cdot \tilde{\mathbf{v}}$ may last tens to hundreds of orbits before changing.

A white line was drawn across the bottom plot in Fig. 8f for when $\tilde{\mathbf{F}} \cdot \tilde{\mathbf{v}} = 0$. If one compares the bottom, rapidly changing plot, to the top plot, one can see that when the average of $\tilde{\mathbf{F}} \cdot \tilde{\mathbf{v}}$ over a short time interval is positive, then $E(t)$ in the top plot increases, and when the average of $\tilde{\mathbf{F}} \cdot \tilde{\mathbf{v}}$ over a short time interval is negative, then $E(t)$ decreases. This is similar to the $n = 1$ resonance situation, but also significantly different in that here, the average over many plus and minus fluctuations of the power $\tilde{\mathbf{F}} \cdot \tilde{\mathbf{v}}$ is the key entity that leads to changes in $E(t)$. Averaging over these fluctuations enabled the analytic predictions to be carried out of $\varepsilon_{\text{crit},n}$ in Sec. IV of the main article (*e.g.*, see Table 1 and Fig. 7).

In the main article, a similar situation was shown to occur for an $n = 3$ subharmonic resonance (*e.g.*, see Figs. 3 and 4). Shortly, in this supplemental document, we will also see similar situations for $n = 4, 5, 6$. More specifically, $\omega_3 = \frac{1}{3}\omega_1$, $\omega_4 = \frac{1}{4}\omega_1$, $\omega_5 = \frac{1}{5}\omega_1$, etc., where $\omega_1 = \frac{f_1}{2\pi}$ is the net angular frequency of the CP wave, f_1 is the CP wave's frequency, $\omega_3 = \frac{f_3}{2\pi}$, $\omega_4 = \frac{f_4}{2\pi}$, $\omega_5 = \frac{f_5}{2\pi}$, etc., and f_3, f_4, f_5 , etc., are the net orbital frequencies of the

classical electron orbit. We will see that similar scenarios to our $n = 2$ example will play out. A unique value of $\varepsilon_{\text{crit},3} \approx 0.669$ occurs for all $n = 3$ subharmonic resonances, no matter the orbital resonance size. For $n = 4$, the basic behavior will again hold, but now $\varepsilon_{\text{crit},4} \approx 0.732$. These points will be brought out, with some caveats, and analyzed in more detail.

Regarding the $n = 3$ situation which was discussed in the main article, including Figs. 3 and 4, an additional interesting figure for this situation is shown here in Fig. 9. Figure 9 shows a “magnified” view of the a vs. t curves during the period from when the $n = 3$ resonance changes into a decaying orbital trajectory. As can be seen, two other resonances, not really visible in Fig. 3, are passed through, namely, the $a_2 = a_1 2^{2/3} = 0.4762 \text{ \AA}$ and $a_1 = 0.3 \text{ \AA}$ resonance points. The conditions imposed by A , ε , α at these resonance points were insufficient to significantly delay further decay, unlike the $a_3 = 0.6240 \text{ \AA}$ point. For sustained resonance to occur, the orbit must have a close correlation in phase with the CP wave. This only occurred here at the $n = 3$ subharmonic resonance point, not the $n = 2$ and $n = 1$ points, although signatures of these resonance positions are clear to see, which is the reason for showing this figure.

To help illustrate these behaviors further, Fig. 10 shows how r vs. t occurs for the $a_1 = 0.5 \text{ \AA}$ case in Fig. 5. As the eccentricity starts to increase once subharmonic resonance is reached, the orbit changes from circular to elliptical character, with a minimum radius of $(1 - \varepsilon)a$ and a maximum radius of $(1 + \varepsilon)a$ in each orbit. At the point of onset of decay, with $a_2 = a_1 2^{2/3} = 0.7937 \text{ \AA}$ and $\varepsilon_{\text{crit},n} \approx 0.554$, then $r_{\text{min}} = 0.354 \text{ \AA}$ and $r_{\text{max}} = 1.234 \text{ \AA}$, agreeing fairly nicely with the data shown in Fig. 10. Changing the CP amplitude A does not significantly alter the envelope of the huge number of orbit fluctuations in Fig. 10, nor does it influence the final value of $\varepsilon_{\text{crit},2}$, but it does alter the length of time that the subharmonic resonance lasts before decay sets in again.

Figure 11 provides further information on the unusual behavior of these subharmonic resonances. Six plots are shown of θ_0 vs. t for the corresponding case of Fig. 8, where $a_1 = 0.6 \text{ \AA}$ and $a_2 = a_1 2^{2/3} = 0.9524 \text{ \AA}$, $a_{\text{initial}} = 1.08 \text{ \AA}$, but where A takes on six different values of 100, 500, 1000, 5000, 10,000, and 50,000 statvolt/cm. Here, θ_0 increases the largest amount when $A = 50,000$ statvolt/cm (of the six situations examined), with about 57,000 radians change occurring for θ_0 , when in subharmonic resonance. If we were to carry out a similar set of simulations, with the same values of A , but when $a_1 = 0.5 \text{ \AA}$ and $a_2 = 0.7937 \text{ \AA}$,

as in Fig. 10, we would see about 33,500 radians being the maximum when $A = 50,000$ statvolt/cm, and if we were to examine a yet smaller semimajor case, when $a_1 = 0.4 \text{ \AA}$, then about 17,000 radians would occur during resonance when $A = 50,000$ statvolt/cm.

III. SIMULATIONS TO HELP SUPPORT APPROXIMATIONS IN SEC. IV OF MAIN ARTICLE

Two of the key approximations used in Sec. IV of the main article, were (1) $E = \frac{1}{2}m\tilde{\mathbf{v}}^2 - \frac{e^3}{r} \approx -\frac{e^2}{2a}$, and (2) $L_z = mr^2\dot{\theta} \approx e(am)^{1/2}(1 - \varepsilon^2)^{1/2}$. Figures 12a,b,c address part of this concern by showing a typical comparison in each of these two approximations, based on conditions used in Fig. 8. As can be seen, the approximations are indeed excellent; although these approximations do depend on quantities like A , in particular, still, these approximations shown in Fig. 12 were fairly typical for the situations examined here.

Another point mentioned in the main paper had to do with taking a time average for Eq. (25) in the main article, reproduced here as:

$$\frac{d}{dt} \left[e(am)^{1/2}(1 - \varepsilon^2)^{1/2} \right] \approx -\frac{\tau e^2 \dot{\theta}}{r} + e r A \cos(\theta - \omega_1 t - \alpha) \quad . \quad ((25))$$

However, as can be seen in Fig. 12a, the short time average of the left side certainly does not always equal zero when in resonance, at least not until the resonance has lasted until nearly the end, when orbital decay sets in. As said in the main article, “The orbit becomes more and more elliptical throughout the evolution of the subharmonic resonance, so ε increases on average, with small oscillations superimposed. When ε reaches its maximum, , as in Figs. 1 and 3, then the time rate of change of $\langle \varepsilon \rangle$ is essentially zero. This is the point we are interested in, as this involves the value of $\varepsilon_{\text{crit},n}$.”

Figures 12a and 12c show how $L_z \approx e(am)^{1/2}(1 - \varepsilon^2)^{1/2}$ behaves during subharmonic resonance, namely, it decreases until flattening out when orbital decay sets in. At this point, as mentioned in the main article, $\langle \frac{d}{dt} L_z \rangle \approx 0$.

However, there is a caveat here. Many of the simulations in the main article produced an agreement between simulation and analytic prediction of $\varepsilon_{\text{initial}}$ to four digits, some to three digits, and several, such as for $n = 4$ and 5, to only two digits. Several investigations were carried out to better understand this range of agreement. These investigations involved variations in A , α , a_{initial} , and $\varepsilon_{\text{initial}}$. The last two variables seemed to have the largest

effect on $\varepsilon_{\text{crit},n}$. In particular, if the electron’s orbit is started at a_n , or just slightly larger than this value, it turns out that the resonant state will not fully evolve to the situation where L_z relaxes to the condition where $\frac{d}{dt}L_z \rightarrow 0$, as in Fig. 12a. However, in the analytical derivation of $\varepsilon_{\text{crit},n}$ in Sec. IV of the main article, this assumption was made, or rather that $\langle \frac{d}{dt}L_z \rangle \approx 0$ at the onset of orbital decay. This assumption turns out to be not quite true in general, and can lead to a small difference with the predictions of Table 1.

Figure 13a illustrates this last point for an $n = 2$ situation. Several related examples were carried out, but the results were all similar. If a_{initial} is close to a_n , the resonance point, the transition from resonance to decay will occur before $\langle \frac{d}{dt}L_z \rangle$ reaches zero. For the examples checked here, once a_{initial} is larger than a_n by only 0.05 Å to 0.10 Å or more, then the approximation of $\langle \frac{d}{dt}L_z \rangle \approx 0$ at the point of decay is valid. Otherwise, particularly starting right at a_n , does not provide enough time for the orbital dynamics to evolve to a condition of $\langle \frac{d}{dt}L_z \rangle \approx 0$ at the point of decay. Figure 13b illustrates how this behavior propagates to $\varepsilon_{\text{crit},n}$, namely, by again making a_{initial} larger than a_n by only 0.05 Å to 0.10 Å or more, then the value of $\varepsilon_{\text{crit},n}$ becomes essentially independent of a_{initial} and falls into agreement with the prediction in Sec. IV of the main article.

Figure 13c shows this effect upon the resonance point a_n . As can be seen, and as expected, there is little effect here; despite the starting point $a_{\text{initial}} > a_n$, the resonances all end up at the subharmonic resonance point a_n .

The effect of changing the initial eccentricity is somewhat similar. Both a_{initial} and $\varepsilon_{\text{initial}}$ can change the value of $\varepsilon_{\text{crit},n}$ from the results in Table 1, as well as change whether the classical electron is even “caught” in a long subharmonic resonance or not. For example, if $\varepsilon_{\text{initial}}$ is too large, then likely no “catch” will be made at all. As might be expected, the likelihood of a catch really comes down to how close in phase the orbit and CP wave can be established when averaged over time.

IV. SIMULATION EXAMPLES OF $n = 4, 5, 6$ SUBHARMONIC RESONANCES

As we go through the $n = 4, 5$, and 6 subharmonic resonance examples in this section, some of the concerns brought up in the previous section will be discussed. In particular, we will note (1) the need to change the initial conditions for a_{initial} and $\varepsilon_{\text{initial}}$ on some of these examples in order to obtain the “catch,” (2) how finding these conditions is nontrivial, and

(3) how these choices change the degree of agreement with Table 1.

Figure 14a shows catching the electron in an $n = 4$ state. The center of the eccentricity curve is good through the first two digits of the predicted value from Table 1 (*i.e.*, $\varepsilon_{\text{crit},4} \approx 0.73$), but not better than two digits, which is a bit interesting since the $n = 5$ case was similar, but the $n = 6$ comes closer, and certainly the opening $n = 2$ example in Sec. I of the main article was far better. However, based on the analysis in the last section, we have a good idea as to the cause of the degree of agreement in these cases.

Figure 14b focuses on the point of decay in Fig. 14a. a vs. t is plotted in this narrow time region, showing that as the electron decays, a net of four, very clear subharmonic resonances are passed through. The values of $a_n = a_1 n^{2/3}$ are extremely precise. Here, as in most cases, only one clear “catch” is made (*i.e.*, at $n = 4$, but not at the subsequent $n = 3, 2$, or 1 resonance points).

The other interesting feature of Fig. 14b, is that additional small signs of resonances can be observed that have not been discussed yet. In terms of the a vs. t curve, these are far less noticeable than the ω_1/n subharmonic resonances discussed in this article. Their values are midway between the primary and subharmonic resonances with periods T_1 times 1, 2, 3, 4 ($T_1 = \frac{2\pi}{\omega_1}$ is the CP wave period), and have precise values T_1 times $\frac{3}{2}$, $\frac{5}{2}$, and $\frac{7}{2}$. Such resonances of the type $\frac{n}{m}\omega_1$, where n and m are integers, have been studied by others for one dimensional oscillators. Here we see their presence, but clearly their effect on the orbit is small compared to the ω_1/n resonances.

Figure 14c shows a case where a decaying electron orbit is caught in a $n = 5$ subharmonic resonance, while Fig. 14d shows a similar case for $n = 6$. The “caveats” to mention here is that none of these examples of $n = 4, 5, 6$ “catches in Fig. 14, were easy to come by. As just discussed, resonance signs of “blips” in an a vs. t decaying curve are easy to spot, such as in Fig. 9 or 14b, and can be obtained for high numbers like $n = 10$, and higher. However, it appears nontrivial for $n \geq 4$ to obtain conditions such that the electron doesn’t just decay through the resonance, but rather hangs for a substantial time at a_n . Evidently, the higher the value of n , to some extent the harder it is to find the right condition to make the “catch” happen.

For $n = 2$ or 3, the key concern seems to be to make A larger than some critical value, as discussed in [7]. For the $n = 4$ case here, besides the value of A (here 75,000 statvolt/cm), the initial eccentricity had to be about 0.05, and the electron had to start very close to a_4 .

For the $n = 5$ case in Fig. 14c, the initial value of ε had to be increased to 0.1 before the “catch” was accomplished. The same was true for the $n = 6$ case in Fig. 10d, but here the electron needed to be “dropped” at a slight “height” above a_6 before the “catch” could be accomplished. Indeed, starting at $a_6 = 0.25 \times 6^{2/3} \text{ \AA} = 0.8255 \text{ \AA}$, resulted in the electron not being caught at the $n = 6$ point, nor at the next $n = 5, 4,$ and 3 resonance points, but decayed right past all of these before finally being caught at $n = 2$. The resonance “blips” were observable, but the conditions were not such as to make the “catch.” Changing the starting a value (*e.g.*, a_{initial}) just slightly, from $a_6 = 0.8255 \text{ \AA}$ to 0.83 \AA , however, enabled the $n = 6$ catch shown in Fig. 14d.

This article does not address why such slight changes can have such large effects. Physically speaking, the reason is certainly clear, as the answer goes back to Fig. 8f concerning $\tilde{\mathbf{F}} \cdot \tilde{\mathbf{v}}$ vs. t . When the CP wave can provide a positive energy input to the trajectory, on average, over many orbits, then the decaying effect of the constantly acting radiation reaction can be compensated. $\tilde{\mathbf{F}} \cdot \tilde{\mathbf{v}}$ alters the orbit in subtle ways, providing a statistical impact of positive and negative energy input. A positive correlation effect between $\tilde{\mathbf{F}}$ and $\tilde{\mathbf{v}}$ can keep the orbit in a somewhat stable resonance state. Predicting precise effects from A , initial a , initial ε , and α , has apparently greater sensitivity for higher values of n .

Thus, some mention and examples have been provided of the often subtle, but important impact on obtaining sustained subharmonic resonances due to different values of A , initial a , initial ε , and α . Regarding α , the angle between $-e\tilde{\mathbf{E}}_{\text{CP}}$ and $\frac{d}{dt}\tilde{\mathbf{z}}$ at $t = 0$, we have not discussed its effect much yet, but it can have a fair impact on the length of time that the semi-stable resonances lasts, as covered in some detail in [5] for $n = 1$. Not surprisingly, for $n \geq 2$ resonances, similar effects occur, as α can effect how long correlation can exist between the electron’s motion and the CP wave.

V. BRIEF SUMMARY OF INFORMATION IN THIS DOCUMENT

The supplemental material presented here went over more detailed information concerning $n = 2$ and $n = 3$, than was presented in the main article. The approximations (1) $E = \frac{1}{2}m\tilde{\mathbf{v}}^2 - \frac{e^3}{r} \approx -\frac{e^2}{2a}$, and (2) $L_z = mr^2\dot{\theta} \approx e(am)^{1/2}(1 - \varepsilon^2)^{1/2}$ were then examined, as these were an important part of the derivation in Sec. IV of the main article in deducing $\varepsilon_{\text{crit},n}$ in Table 1 and Fig. 7 of the main article. Next, an understanding was gained regarding

that $\langle \frac{d}{dt} L_z \rangle \approx 0$ is not always true if a_{initial} is too close to a_n , since the classical electron's angular momentum does then not have sufficient time to relax to the condition of $\langle \frac{d}{dt} L_z \rangle \approx 0$ when orbital decay eventually sets in. This results in changes in accuracy of Table 1, since $\langle \frac{d}{dt} L_z \rangle \approx 0$ when orbital decay sets in, was assumed in the derivation in Sec. IV. Clearly this assumption could be improved up, but was not done here. Despite this observation, Table 1 still seems fairly close to two digits of accuracy, or as high as four, as seen in some of the examples here.

Finally, subharmonic resonance examples for $n = 4, 5, 6$ were shown in Sec. 4. A discussion was given as to why they were harder to deduce than the evidently easier examples of $n = 2$ and 3. Also, some further interesting properties were found for these subharmonic resonances, such as some weak resonances of the type $\frac{n}{m}\omega_1$.

Fig. 8 All of the Figs. 8a to 8f were carried out under the same conditions, namely, $a_1 = 0.6 \text{ \AA}$, ω_1 for the CP wave was $\omega_1 = \left(\frac{e^2}{ma_1^3}\right)^{1/2}$, the orbit began at $a_{\text{initial}} = 1.08 \text{ \AA}$ in a circular orbit, so $\varepsilon_{\text{initial}} = 0$, $A = 1000 \text{ statvolt/cm}$, and $a_2 = a_1 2^{2/3} \approx 0.9524 \text{ \AA}$, and $\alpha = 0$ in (12) and (13).

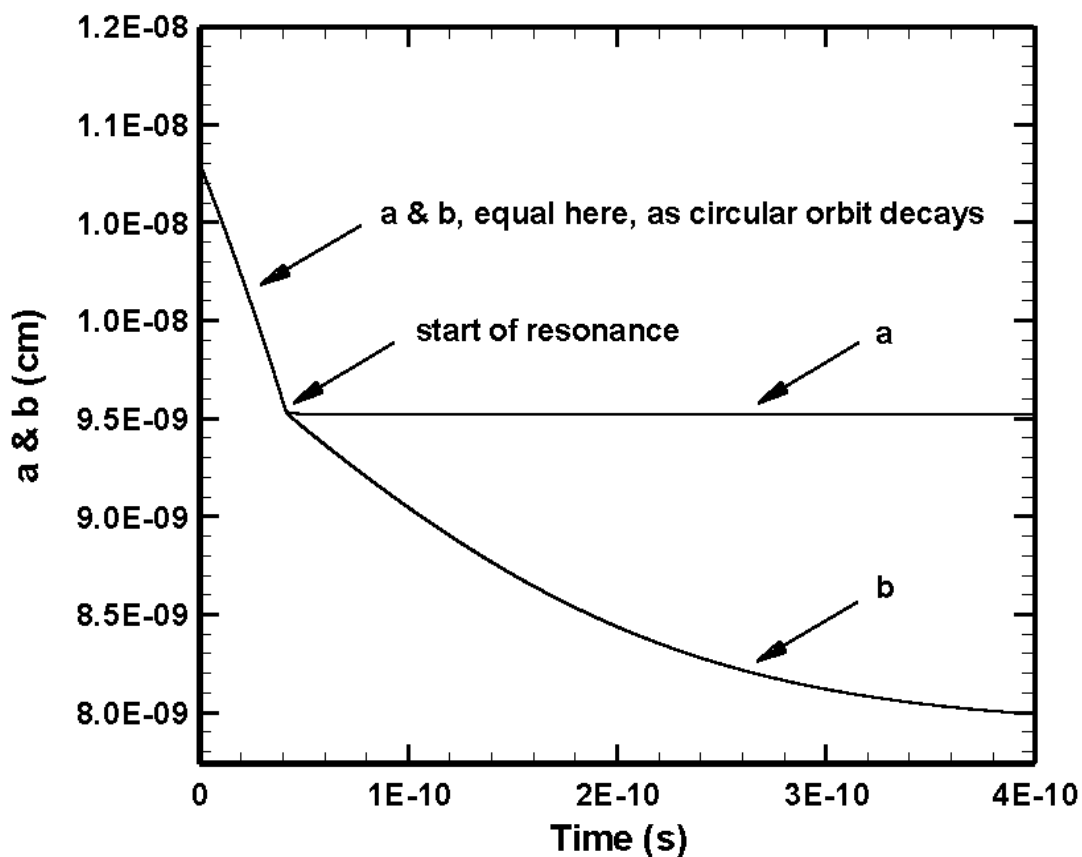


Fig. 8a Plots of $a(t)$ and $b(t)$ vs. t , for the start of an $n = 2$ subharmonic resonance, shown to the end of the resonance in Fig. 8b. The key points to note are that the orbit initially decays, during which $a = b$, then a sharp change occurs when resonance is reached at $a_2 = a_1 2^{2/3} = 0.9524 \text{ \AA}$, after which a stays flat, while b decreases.

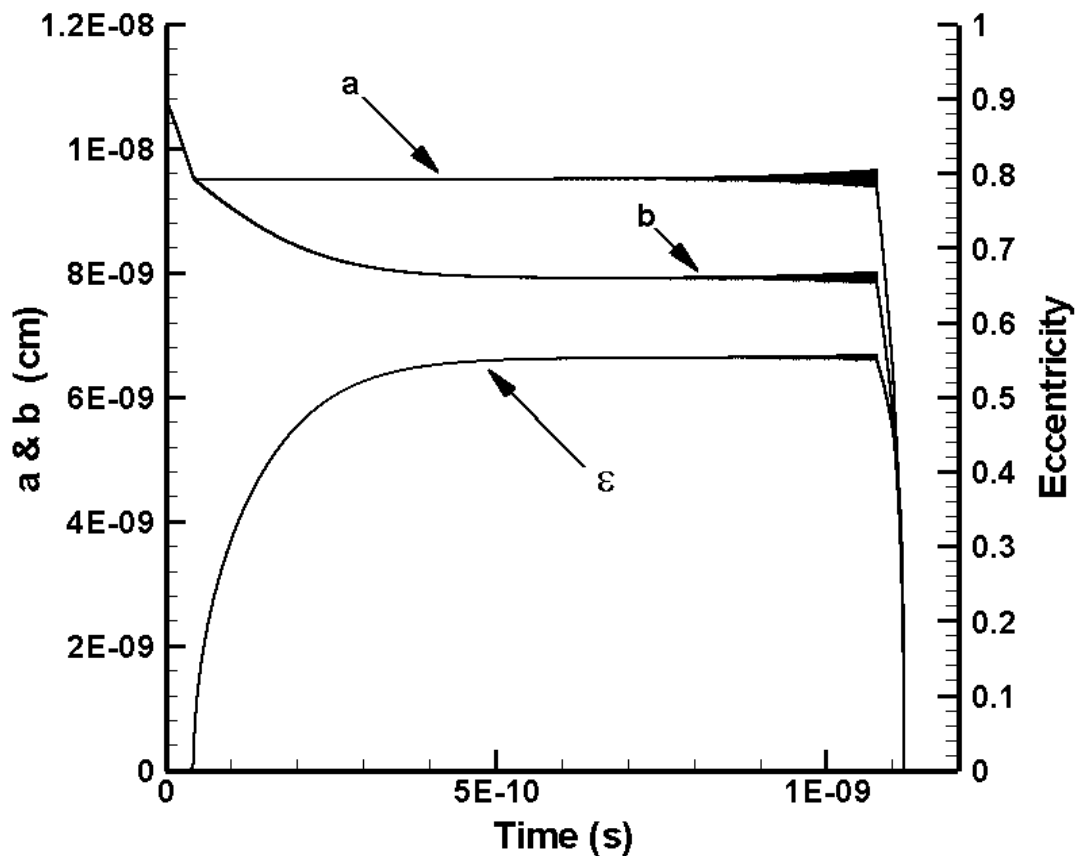


Fig. 8b Plots of a , b , and ε vs. t , from start to finish, where the orbit begins in a decaying circular orbit (Fig. 8a), then proceeds to the start of the $n = 2$ subharmonic resonance, then to the end of this resonance, finally ending in orbital decay. As shown in Sec. IV of the main article, $\varepsilon_{\text{crit},n} \approx 0.5542$ for $n = 2$, is the eccentricity when the transition of orbital resonance to decay occurs.

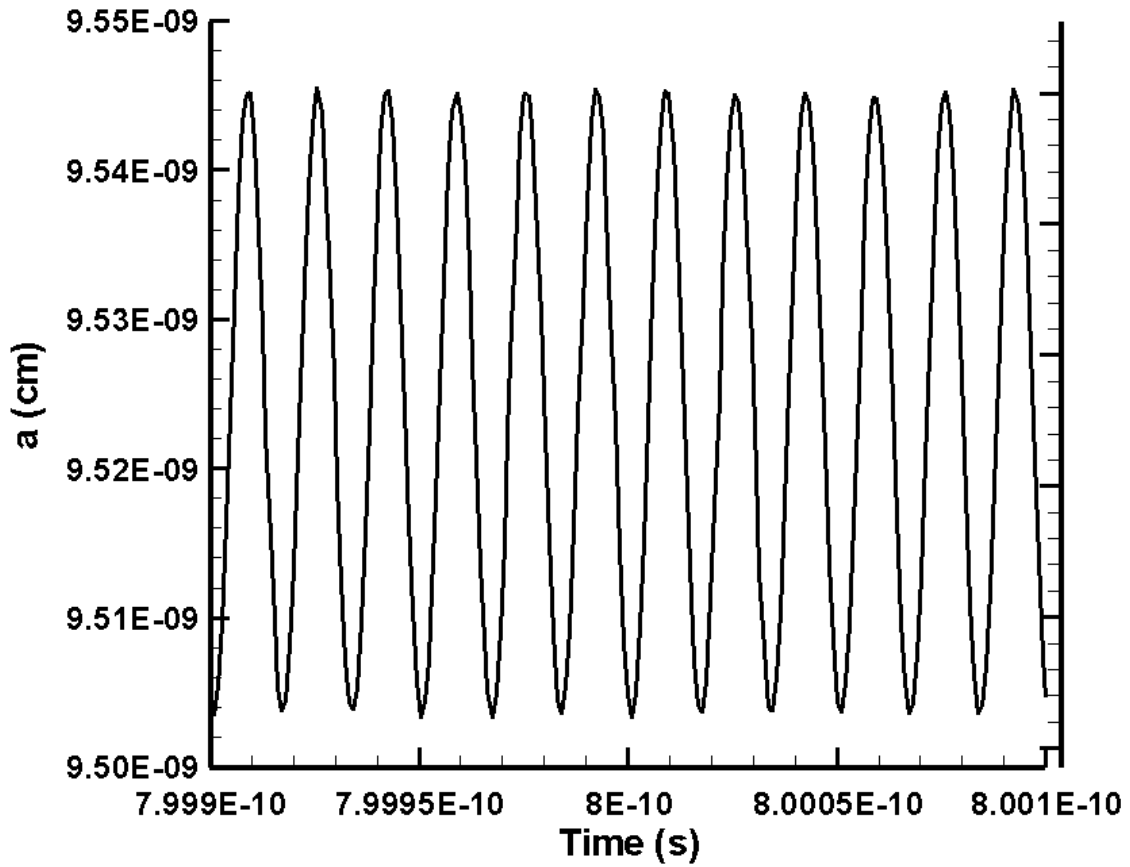


Fig. 8c This plot focuses in on the a vs. t curve in Fig. 8b at about 75% into the subharmonic resonance, at $t \approx 8 \times 10^{-10}$ s. At this scale of the plot, the variation in a looks large, but it is only about a $\pm 0.2\%$ variation in $a(t)$. By the point in Fig. 8b where orbital decay sets in, this variation in $a(t)$ rises to about a $\pm 1.4\%$ variation. However, the larger A is, the larger will be this variation. Aside: for each full oscillation of $a(t)$ in this figure, there are approximately 46 orbital periods at this point in time.

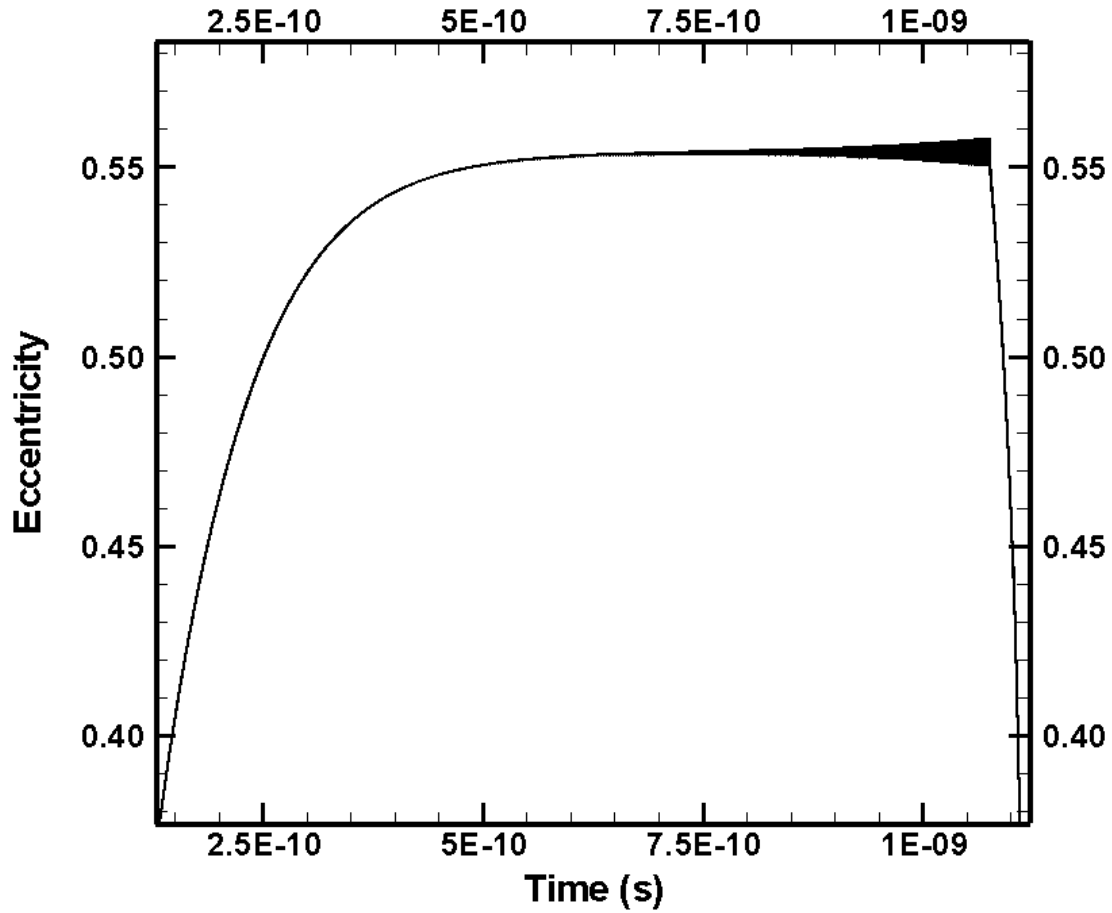


Fig. 8d Plot of $\varepsilon(t)$ vs. t , containing the same information as in the $\varepsilon(t)$ curve in Fig. 8b, but now focusing in at the point leading up to decay and showing more clearly the widening of the curve, until decay sets in. Once $\varepsilon \approx 0.5542$ is reached, ε then rapidly decays toward zero, a circular orbit.

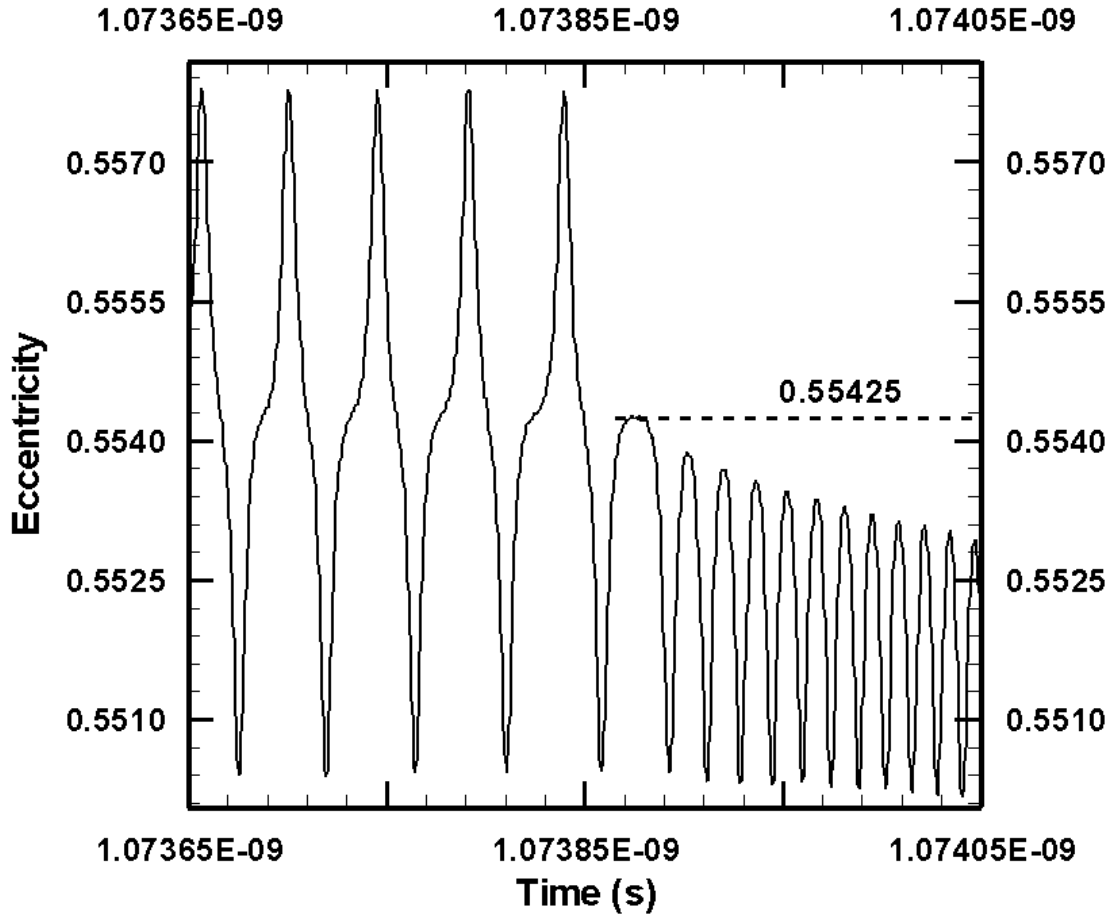


Fig. 8e This plot of $\varepsilon(t)$ vs. t , focuses in at the point where the widening curve in Fig. 8d, changes to a decaying orbit. For $t \lesssim 1.07385 \times 10^{-9}$ s, the oscillations have lower and upper humps that look something like a “pinched” sine wave. However, at $t \approx 1.07385 \times 10^{-9}$ s, the top peaks pinch off entirely, leaving the smaller, decaying oscillations that can be seen for 1.07385×10^{-9} s $\lesssim t$. Similar “signatures” of this behavior also appear for $a(t)$, $b(t)$, and energy and angular momentum. Far to the left of the decay point, the oscillations of these variables look more like Fig. 8c, but the closer to the decay point, the more “pinched” become the peaks and valleys, until decay sets in. The $\varepsilon_{\text{crit},2}$ point noted here, of ≈ 0.5542 , agrees closely with the analytical results of Sec. IV (see, Table 1 and Fig. 7) in the main article.

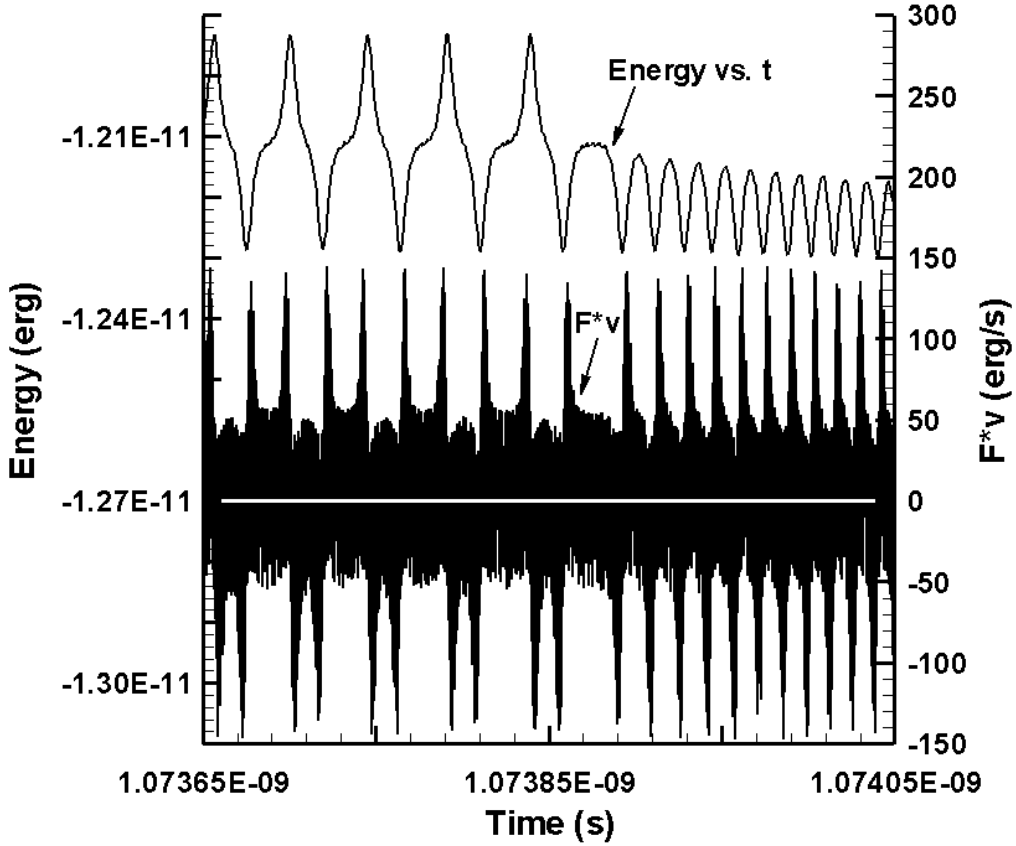


Fig. 8f The top plot is of $E(t) = -\frac{e^2}{r(t)} + \frac{1}{2}m|\tilde{\mathbf{v}}(t)|^2$ (units on left axis) which will be shown later in this supplemental material, to be close to $-\frac{e^2}{2a(t)}$ for the range of values of A considered here in this article. Of course these would be exactly equivalent if the CP wave and radiation reaction were not present. The bottom plot is of $\tilde{\mathbf{F}} \cdot \tilde{\mathbf{v}}$ vs. t (units on right axis), where $\tilde{\mathbf{F}}$ is the sum of the CP wave and radiation reaction forces. This “power” of the work per time by the CP wave and radiation reaction is of course what changes $E(t)$ in the top curve; if these two forces were zero, then $E(t)$ would be a constant and we would be back to a pure Coulombic elliptical orbit that does not change. The fast fluctuations of $\tilde{\mathbf{F}} \cdot \tilde{\mathbf{v}}$ create a complicated scenario, but by averaging in time over short regions, one can see that when $\tilde{\mathbf{F}} \cdot \tilde{\mathbf{v}}$ is more positive than negative, then $E(t)$ increases, and vice versa. The white line indicates when $\tilde{\mathbf{F}} \cdot \tilde{\mathbf{v}} = 0$, to help make it easier to see this last connection. The time span here is the same as in Fig. 8e, so right when the orbit changes from a state of resonance to one of decay.

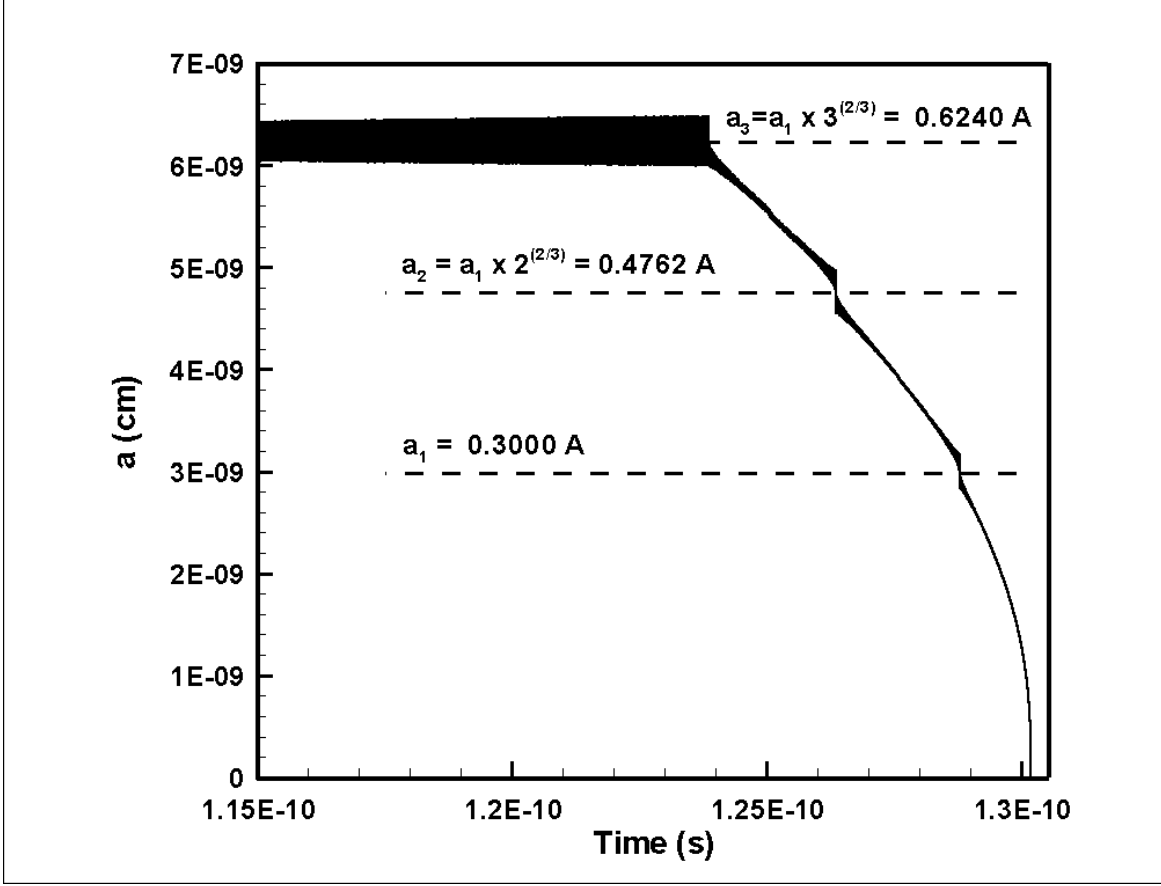


Fig. 9 Here, the $a(t)$ vs. t curve in Fig. 3 of the main article is examined in the very narrow region where the $n = 3$ subharmonic resonance changes to one of orbital decay. Although not visible in Fig. 3, here we see that after the electron leaves the $n = 3$ subharmonic state, it passes through two other resonant states, with conditions of A , ε , α , insufficient to delay decay at these points. These other resonant positions occurred at the $n = 2$ and $n = 1$ positions: $a_2 = a_1 \times 2^{2/3} \text{ \AA} = 0.4762 \text{ \AA}$, and $a_1 = 0.3 \text{ \AA}$. As in Figs. 3 and 4, $A = 35,000$ statvolt/cm, $a_{\text{initial}} = 0.7 \text{ \AA}$, and $\varepsilon_{\text{initial}} = 0$.

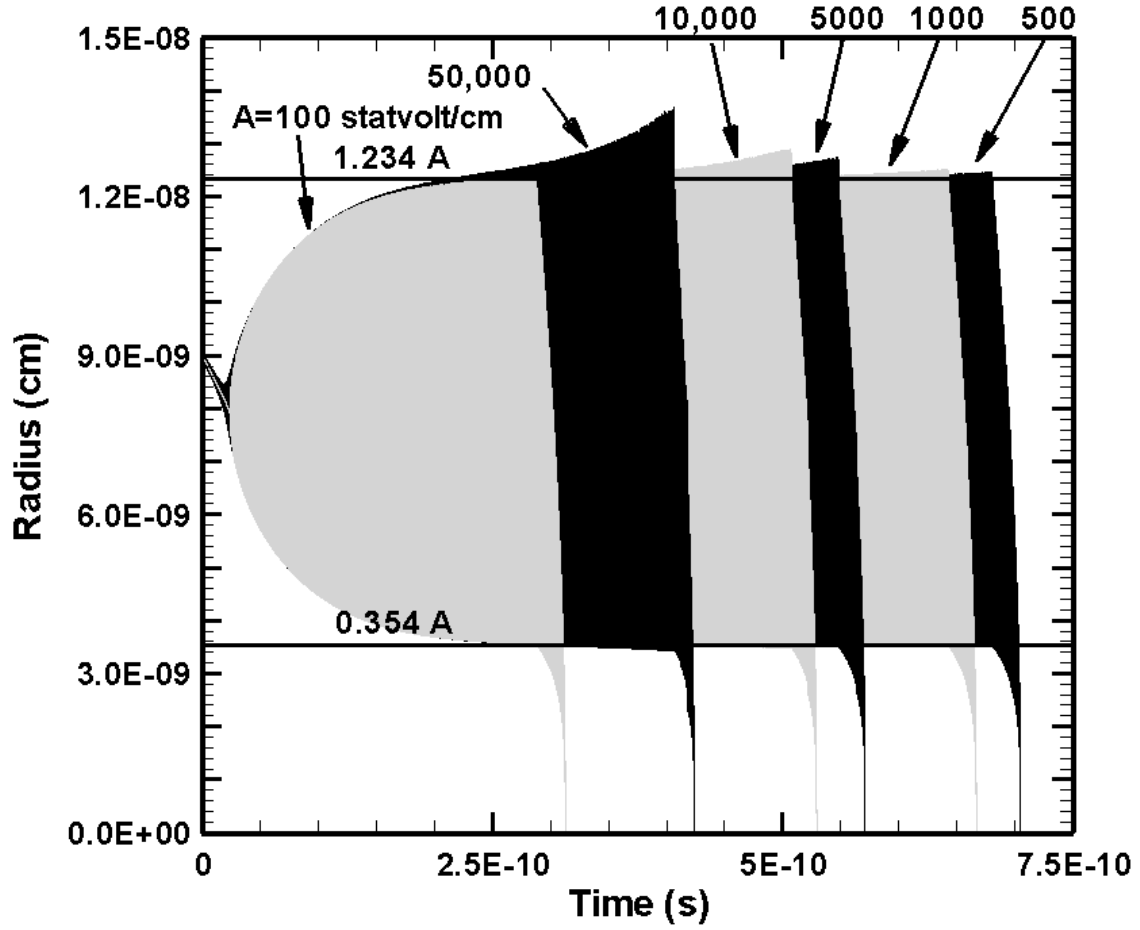


Fig. 10 This figure contains a set of plots of radius versus time, that corresponds to Fig. 5 in the main article, where $a_1 = 0.5 \text{ \AA}$, $a_2 = 0.7937 \text{ \AA}$, and $a_{\text{initial}} = 0.90 \text{ \AA}$. The large radius change is due to the orbit, initially in a circular state, changing to an elliptical state, where the maximum of the eccentricity is about 0.554, and is largely independent of the value of the CP amplitude. The two horizontal lines of 1.234 \AA and 0.353 \AA represent the maximum and minimum of the radius, given that $\epsilon_{\text{max}} \approx 0.554$.

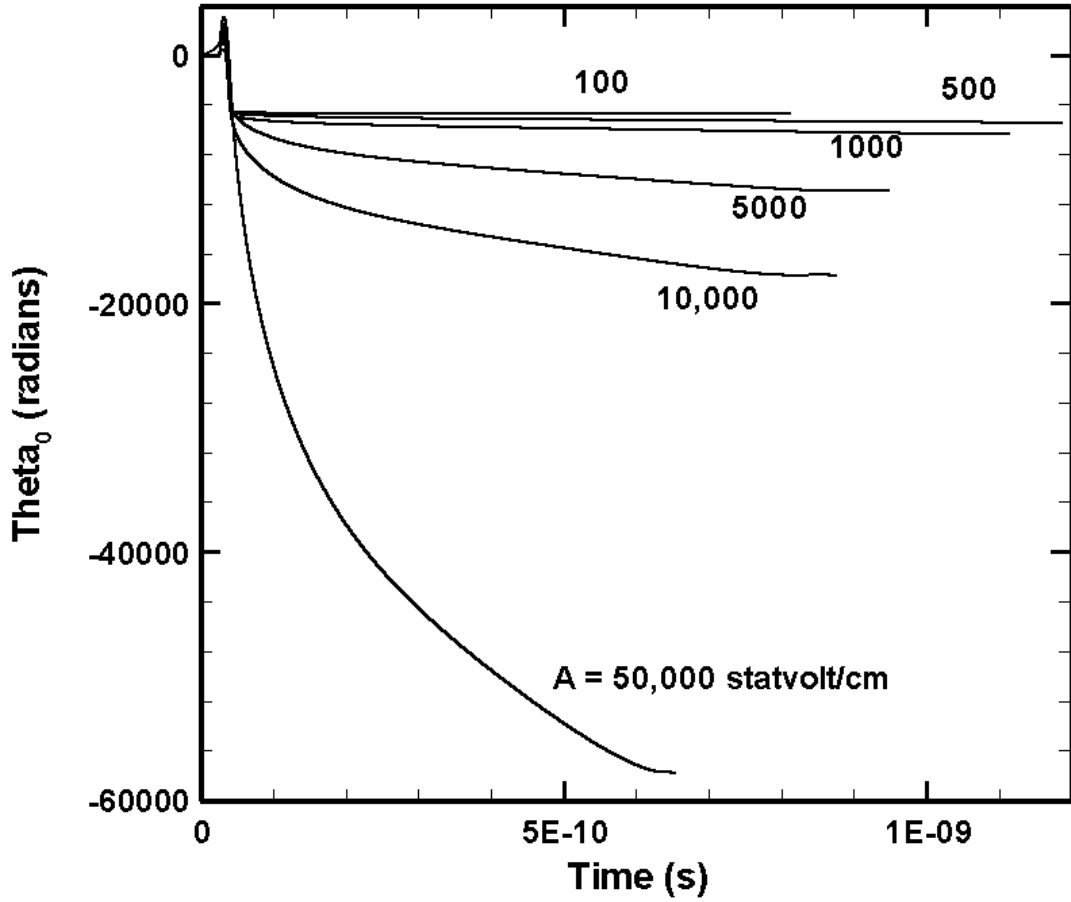


Fig. 11 Plot of θ_0 vs. t when $a_1 = 0.6 \text{ \AA}$, $a_2 = 0.9524 \text{ \AA}$. Six different values of A are used to create the six plots, corresponding to Fig. 8. All trajectories are started in circular orbits with $a_{\text{initial}} = 1.08 \text{ \AA}$. The larger the value of A , the more the elliptical orbit rotates while the classical electron is in the subharmonic resonance state.

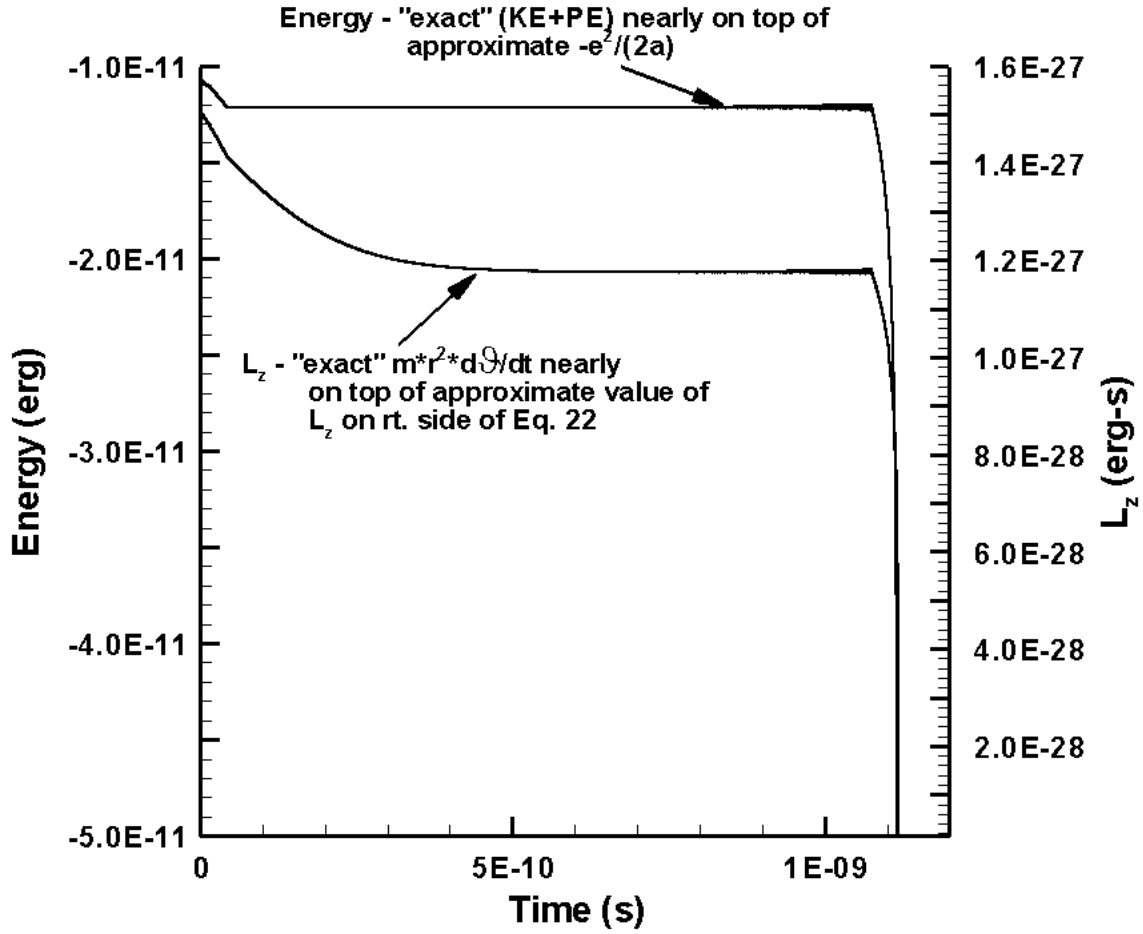


Fig. 12a There are four curves here. The top two involving energy, are essentially on top of each other. Likewise, the bottom two involving angular momentum, are essentially indistinguishable at this view. The top two curves are $E = \frac{1}{2}m\tilde{v}^2 - \frac{e^2}{r}$ and the approximate value $-\frac{e^2}{2a}$. The bottom two are $L_z = mr^2\dot{\theta}$ and the approximate value $e(am)^{1/2}(1-\varepsilon^2)^{1/2}$. The conditions for the simulation are the same as in Fig. 8, namely, $a_1 = 0.6 \text{ \AA}$, $\omega_1 = \left(\frac{e^2}{ma_1^3}\right)^{1/2}$, the orbit began at $a_{\text{initial}} = 1.08 \text{ \AA}$ in a circular orbit, so $\varepsilon_{\text{initial}} = 0$, $A = 1000 \text{ statvolt/cm}$, and $a_2 = a_1 2^{2/3} \approx 0.9524 \text{ \AA}$, and $\alpha = 0$.

Energy - "exact" (KE+PE) versus approximate $-e^2/(2a)$ at the transition point of resonance to decay. The "exact" (KE+PE) has more of a "wiggle" about the approximate value of $-e^2/(2a)$.

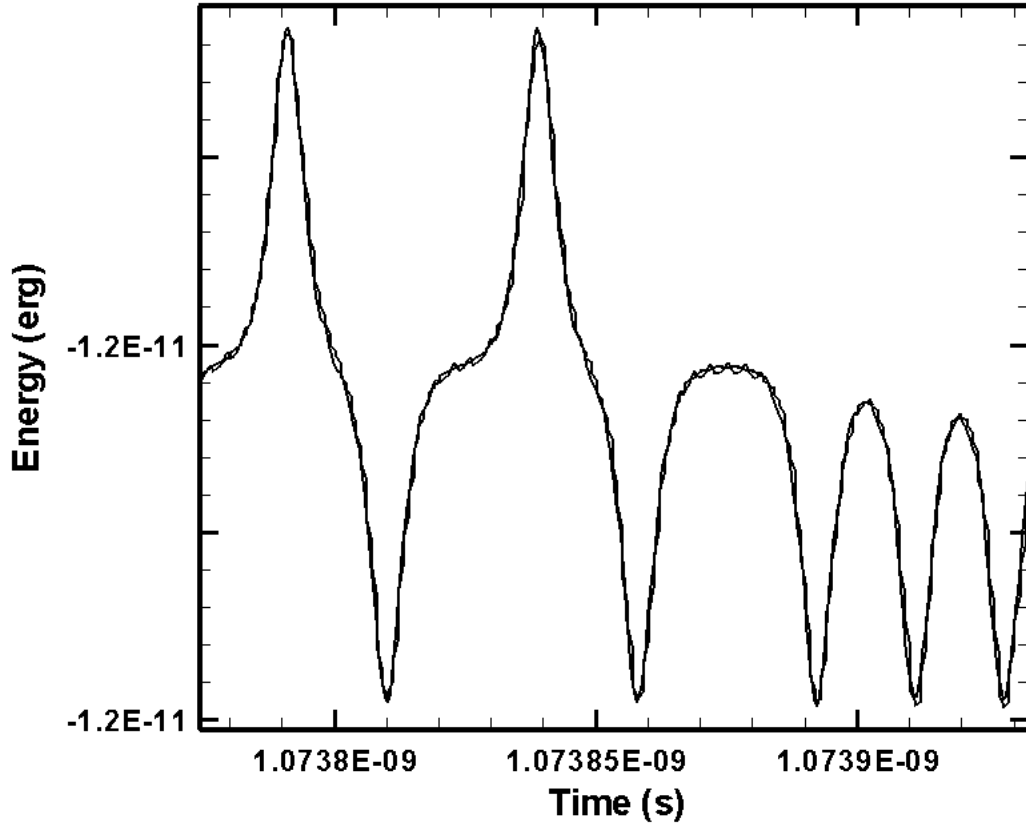


Fig. 12b This plot “zooms” in on the transition point between subharmonic resonance and orbital decay in the top two “energy” curves in Fig. 12a, around $t \approx 1.07385 \times 10^{-9}$ s. The two curves are $E = \frac{1}{2}m\tilde{v}^2 - \frac{e^3}{r}$ and $-\frac{e^2}{2a}$, with the former curve of $\frac{1}{2}m\tilde{v}^2 - \frac{e^3}{r}$ vs. t having the more “wiggles,” for lack of a better description. Clearly, the two curves match each other quite well.

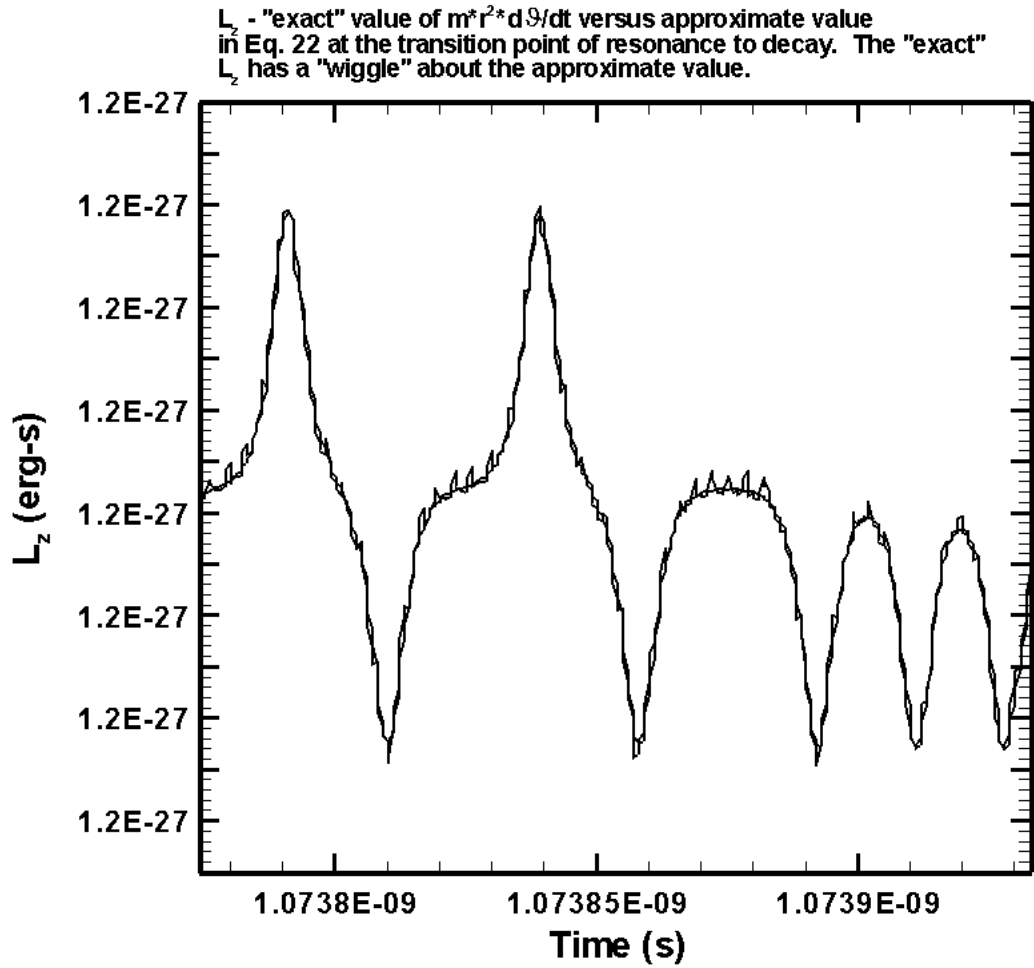


Fig. 12c This plot also “zooms” in on the transition point between subharmonic resonance and orbital decay in Fig. 12a, but for the bottom two “angular momentum curves” in Fig. 12a, around $t \approx 1.07385 \times 10^{-9}$ s. The two curves are $L_z = mr^2\dot{\theta}$ and $e(am)^{1/2}(1 - \varepsilon^2)^{1/2}$, with the former curve of $mr^2\dot{\theta}$ vs. t having the more “wiggles.” Clearly, the two curves match each other quite well.

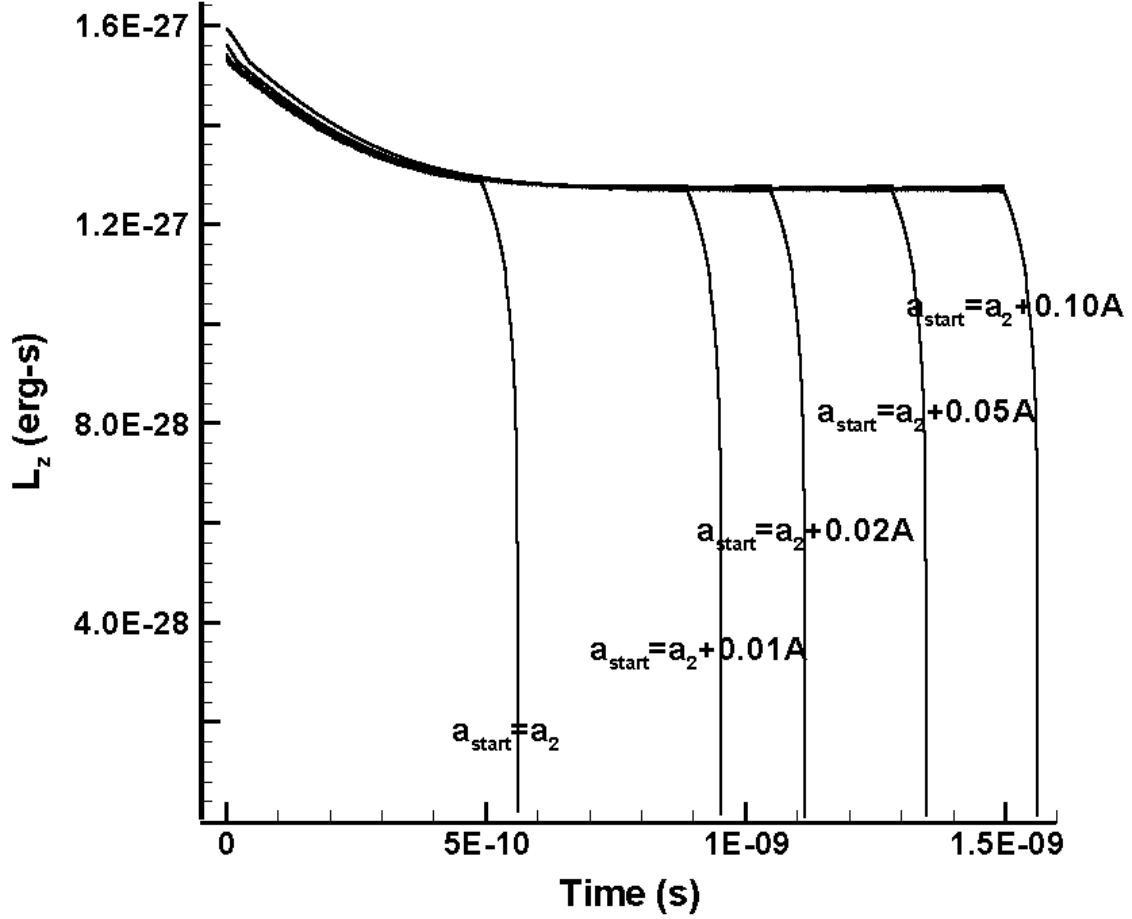


Fig. 13a Five curves are shown here, each a plot of L_z vs. t , but with different starting conditions. In each simulation, $a_1 = 0.7 \text{ \AA}$, ω_1 for the CP wave being $\omega_1 = \left(\frac{e^2}{ma_1^3}\right)^{1/2}$, $a_2 = a_1 2^{2/3} \approx 1.1112 \text{ \AA}$, $A = 1000 \text{ statvolt/cm}$, $\varepsilon_{\text{initial}} = 0$, $\alpha = 0$. The first curve on the left has $a_{\text{initial}} = a_2$, so right at the $n = 2$ resonance. The next four curves to the right, start at $a_2 + 0.01 \text{ \AA}$, $a_2 + 0.02 \text{ \AA}$, $a_2 + 0.05 \text{ \AA}$, and $a_2 + 0.10 \text{ \AA}$, respectively. As can be seen the first curve starting at a_2 does not end with $\langle \frac{d}{dt} L_z \rangle \approx 0$ at the point of decay, although subsequent curves, starting just slightly above a_2 , realize this condition closer and closer.

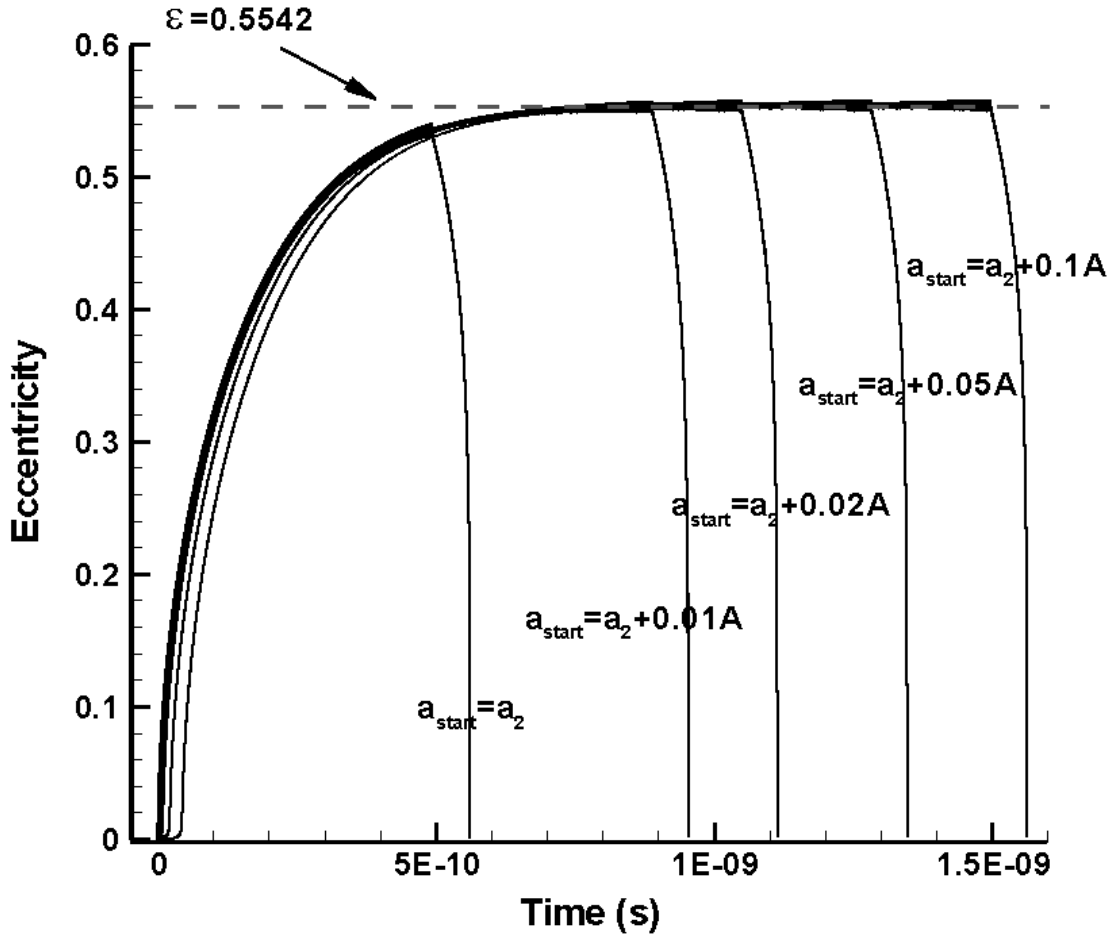


Fig. 13b The same simulation cases as in Fig. 13a are shown here, but now ε vs. t is plotted. The expected $\varepsilon_{\text{crit},2}$ value for $n = 2$ subharmonic resonance as predicted in Table 1 is shown, of $\varepsilon_{\text{crit}} = 0.5542$. As expected by now, the simulation with the classical electron starting at a_2 is a bit off from this predicted value, because of Fig. 13a, which showed that if the electron starts too close to a_2 , then $\langle \frac{d}{dt} L_z \rangle$ will not evolve fully to zero before decay sets in. However, even $a_2 + 0.01 \text{ \AA}$ is enough to change this situation quite a bit.

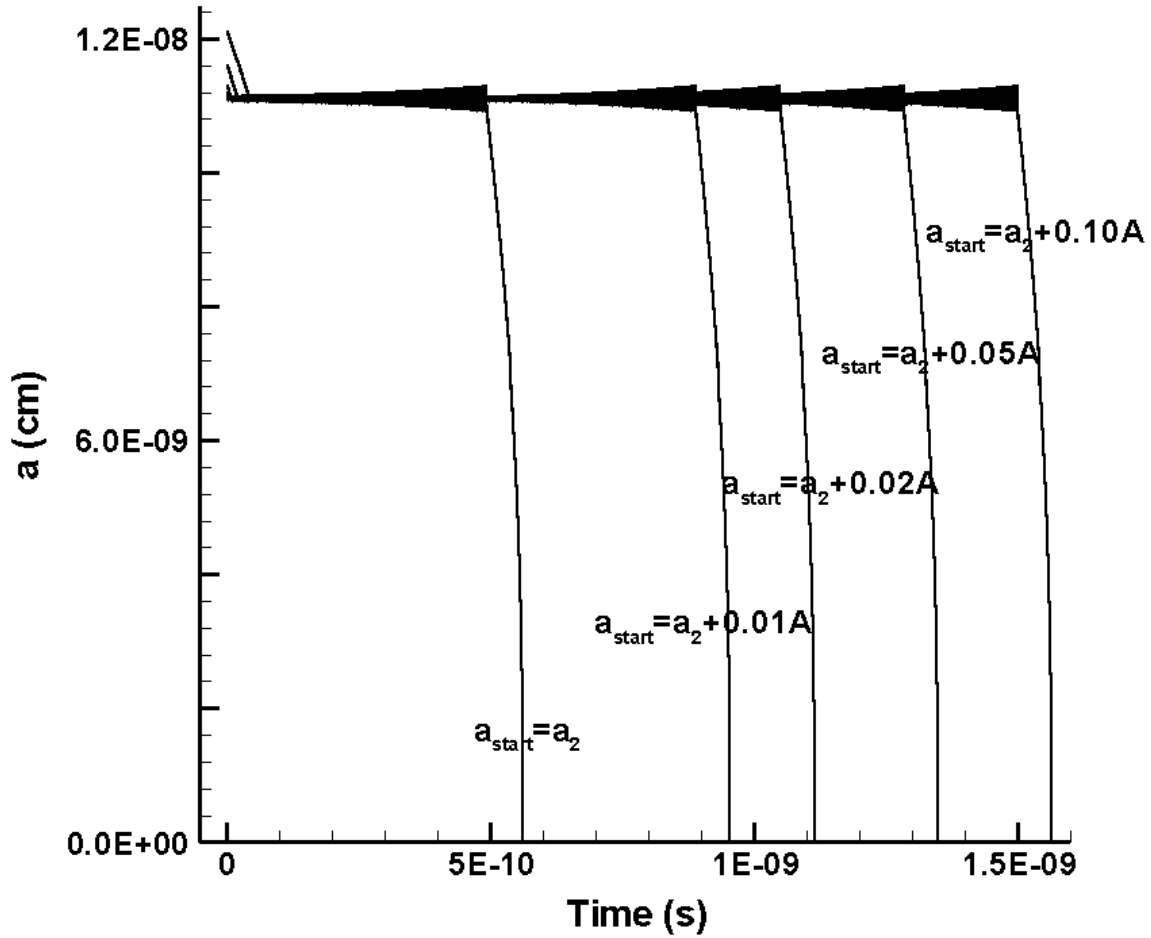


Fig. 13c To put the simulations in Figs. 13a,b in better perspective, $a(t)$ vs. t is shown here for these same five simulation cases. The top lines on the upper left indicate the five starting points in terms of a_{initial} . All curves hit resonance and stay there for a while before decaying, with the longer times before decay increasing the larger x is in $a_{\text{initial}} = a_2 + x$. Sets of simulations for much larger values of x were carried out as well (0.25 \AA , 0.50 \AA , 0.75 \AA) and this monotonic increase of resonance time with x dies out, as might be expected.

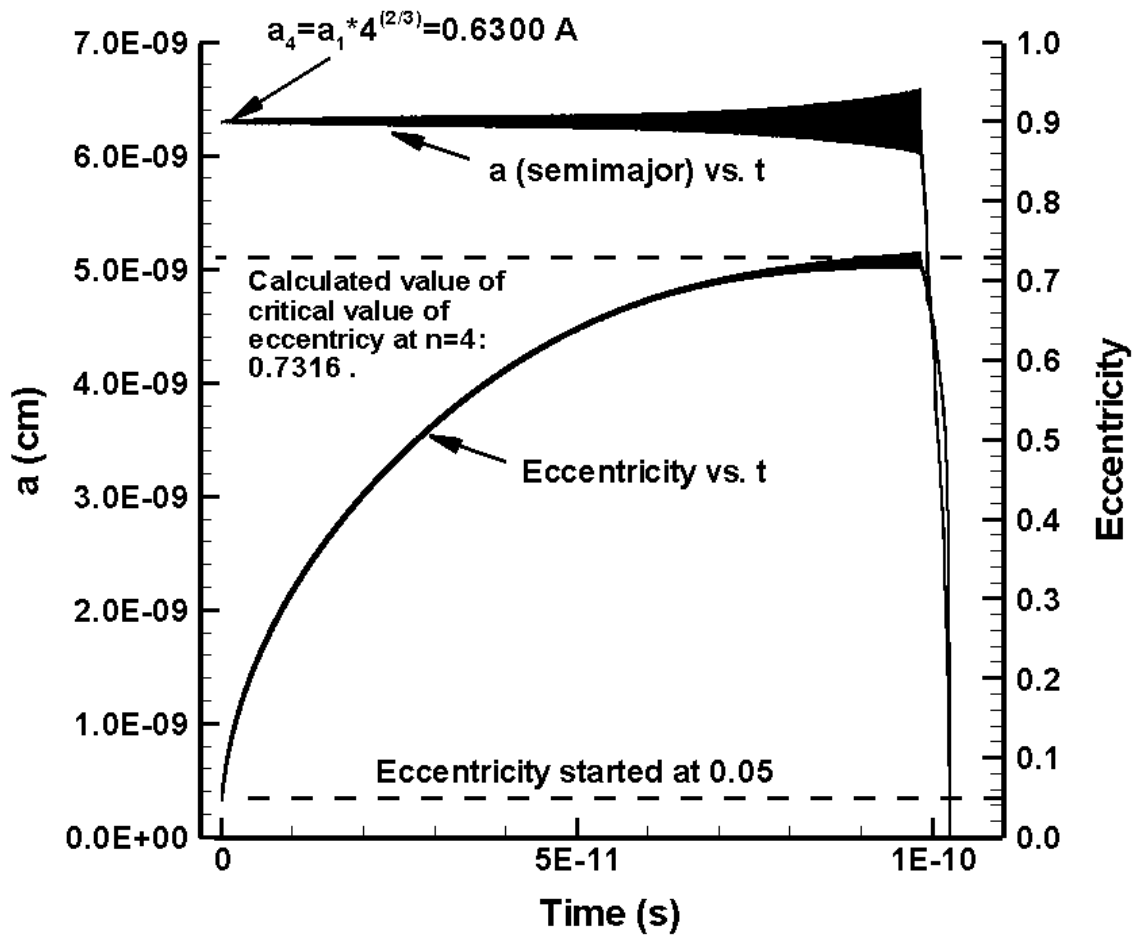


Fig. 14a Here the classical electron was “caught” in an $n = 4$ subharmonic resonance state. $a_1 = 0.25 \text{ \AA}$, $a_4 = a_1 4^{2/3} = 0.6300 \text{ \AA}$. $A = 75,000 \text{ statvolt/cm}$, $\alpha = 0$, $\varepsilon_{\text{initial}} = 0.05$, $a_{\text{initial}} = a_4$. The simulation value of $\varepsilon_{\text{crit},4}$ agreed to the first two digits of the analytically computed value in Table 1 of 0.7316.

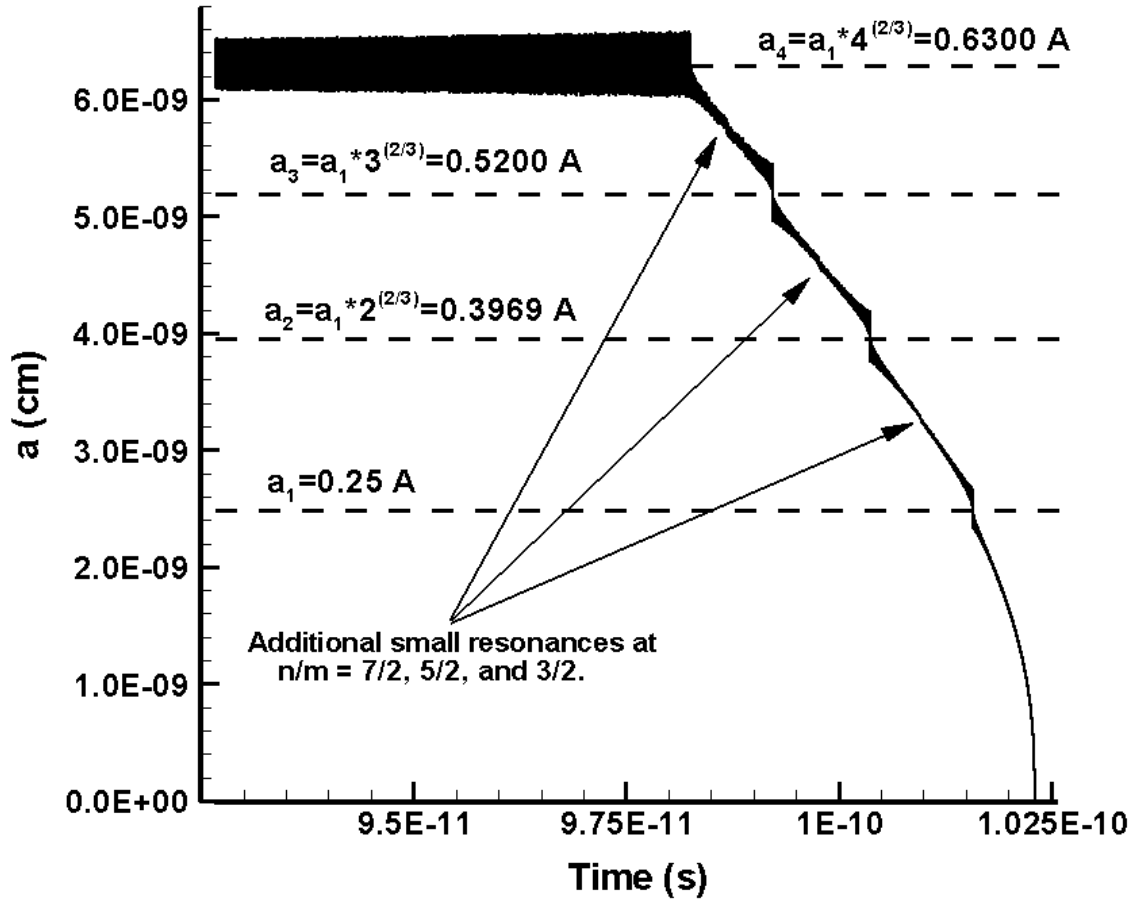


Fig. 14b Here, the very narrow region in Fig. 14a, for the $n = 4$ catch, is examined where the resonance state changes to decay. As can be seen, after leaving the $n = 4$ subharmonic resonance, there are three very clear signs of other resonances, namely at the $n = 3, 2, 1$ states. Their positions agree very precisely with the expected values of $\bar{a}_n = a_1 n^{2/3}$, as shown. None of these resonances have the right conditions to again catch the electron, with one large reason being that during this decay, the orbit is also relaxing from a fairly high eccentricity value of 0.73, and decreasing toward zero. All conditions need to be “right”, including ε , A , α , to create a sustained correlation between $\tilde{\mathbf{F}}$ and $\tilde{\mathbf{v}}$. Also, one can see three interesting, very small resonances, that correspond with $\omega_{\frac{n}{m}} = \frac{7}{2}\omega_1$, $\frac{5}{2}\omega_1$, and $\frac{3}{2}\omega_1$ type resonances. Otherwise, note the similarity between this figure and Fig. 9, which involved an $n = 3$ subharmonic resonance, and where the decay traversed through the $n = 2$ and $n = 1$ states.

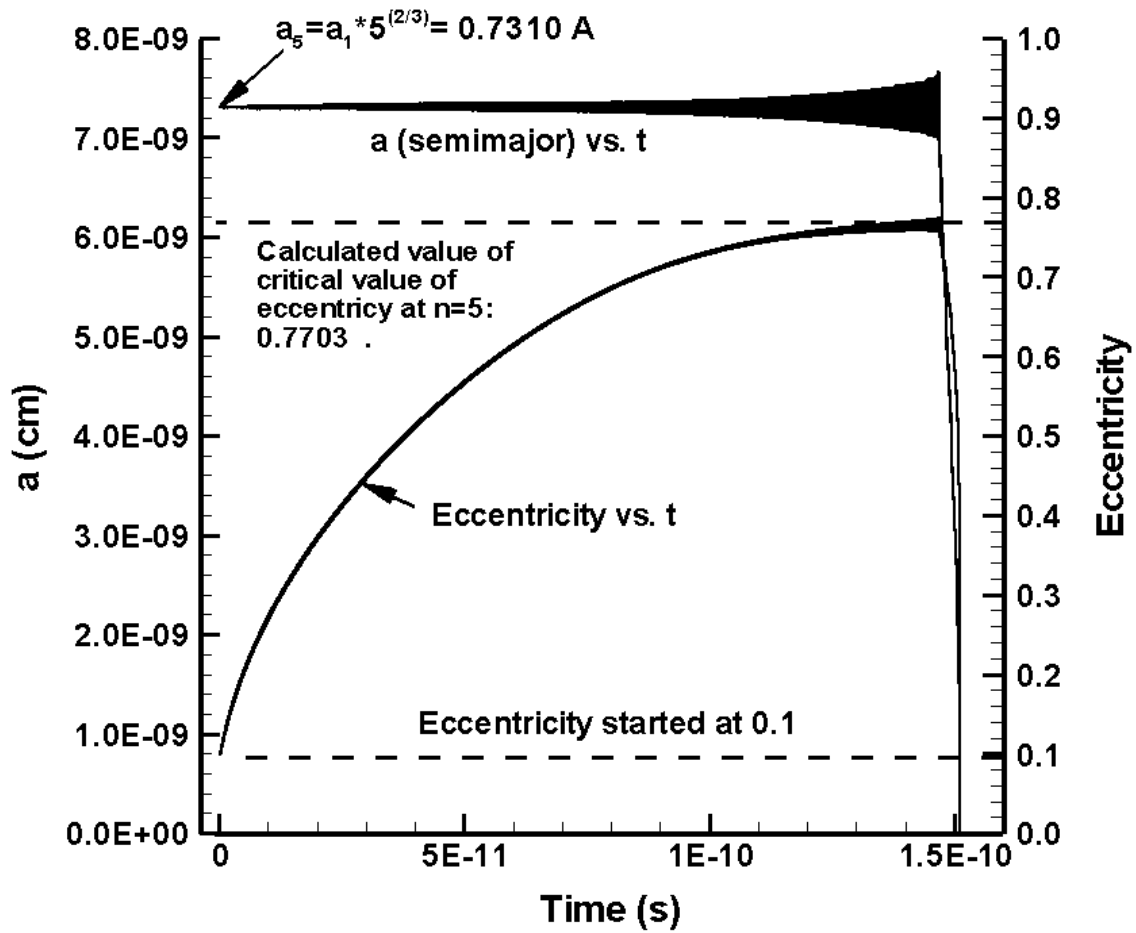


Fig. 14c Here the classical electron was “caught” in an $n = 5$ subharmonic resonance state. $a_1 = 0.25 \text{ \AA}$, $a_5 = a_1 5^{2/3} = 0.7310 \text{ \AA}$. $A = 75,000 \text{ statvolt/cm}$, $\alpha = 0$, $\varepsilon_{\text{initial}} = 0.1$, $a_{\text{initial}} = a_5$. The simulation value of $\varepsilon_{\text{crit},5}$ agreed to within the first two digits of the analytically computed value in Table 1 of 0.7703. If we were to blow up the decay region, as in Fig. 14b, five clear resonant points would be recognizable.

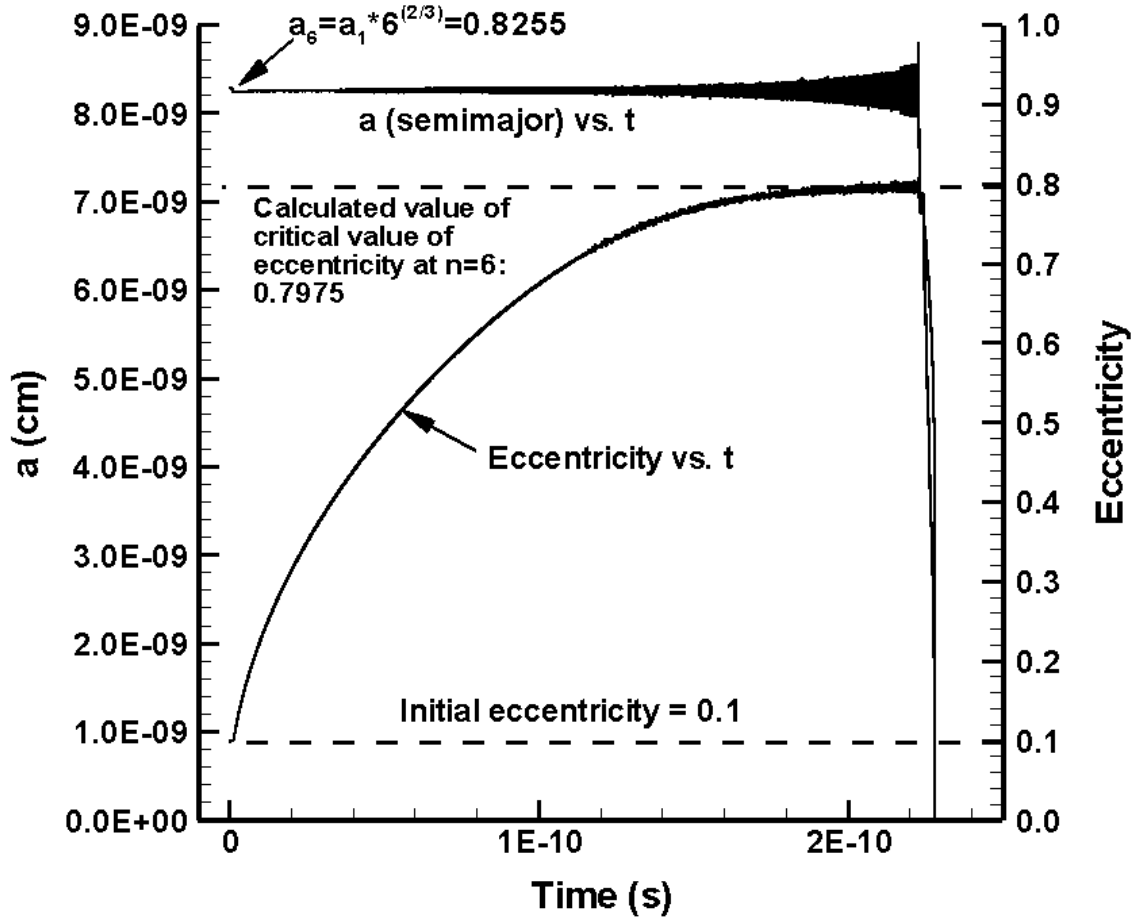


Fig. 14d Here the classical electron was “caught” in an $n = 6$ subharmonic resonance state. $a_1 = 0.25 \text{ \AA}$, $a_6 = a_1 6^{2/3} = 0.8255 \text{ \AA}$. $A = 75,000 \text{ statvolt/cm}$, $\alpha = 0$, $\varepsilon_{\text{initial}} = 0.1$. When using $a_{\text{initial}} = a_6 = 0.8255 \text{ \AA}$, the electron was not caught, but decayed right through this resonant point, as well as the subsequent $n = 5, 4$, and 3 resonant points, before finally being caught in the $n = 2$ state. However, by changing the a_{initial} ever so slightly, from $a_6 = 0.8255 \text{ \AA}$ to 0.83 \AA , then the $n = 6$ state was achieved, as shown here. The simulation value of $\varepsilon_{\text{crit},6}$ agreed to within the first 3 to 4 digits of the analytically computed value in Table 1 of 0.7975. If we were to blow up the decay region, as in Fig. 14b, six clear resonant points would be recognizable.

-
- [1] C. Teitelboim, D. Villarroel, and Ch. G. van Weert. Classical electrodynamics of retarded fields and point particles. *Riv. del Nuovo Cimento*, 3(9):1–64, 1980.
- [2] John David Jackson. *Classical Electrodynamics*. John Wiley & Sons, 2nd edition, 1975.
- [3] D.C. Cole and Y. Zou. Simulation study of aspects of the classical hydrogen atom interacting with electromagnetic radiation: Circular orbits. *Journal of Scientific Computing*, 20(1):43 – 68, 2004.
- [4] D. C. Cole and Y. Zou. Perturbation analysis and simulation study of the effects of phase on the classical hydrogen atom interacting with circularly polarized electromagnetic radiation. *Journal of Scientific Computing*, 21(2):145–172, 2004.
- [5] D. C. Cole and Y. Zou. Analysis of orbital decay time for the classical hydrogen atom interacting with circularly polarized electromagnetic radiation. *Phys. Rev. E*, 69(1):016601–1–12, 2004/01/.
- [6] D. C. Cole and Y. Zou. Simulation study of aspects of the classical hydrogen atom interacting with electromagnetic radiation: Elliptical orbits. *Journal of Scientific Computing*, 20(3):379–404, 2004.
- [7] D. Cole and Yi Zou. Subharmonic resonance behavior for the classical hydrogen atomic system. *J. Sci. Comput. (USA)*, 39(1):1 – 27, 2009/04/.